

## **$^{228}\text{Ra}/^{226}\text{Ra}$ and $^{226}\text{Ra}/\text{Ba}$ ratios in seawater and particles at the OFP site in the western Sargasso Sea near Bermuda**

van Beek P.<sup>1,\*</sup>, François R.<sup>2,3</sup>, Conte M.<sup>2,4</sup>, Reyss J.-L.<sup>5</sup>, Souhaut M.<sup>1</sup>, Charette M.<sup>2</sup>

<sup>1</sup> now at LEGOS (CNRS/CNES/IRD/UPS), Observatoire Midi Pyrénées, 14 avenue Edouard Belin, 31400 Toulouse, France

<sup>2</sup> Woods Hole Oceanographic Institution, Woods Hole MA02543, USA

<sup>3</sup> now at University of British Columbia, Earth and Ocean Sciences Dept, Vancouver, BC, Canada

<sup>4</sup> now at Bermuda Biological Station for Research, Inc., Ferry Reach St Georges GE01 Bermuda

<sup>5</sup> Laboratoire des Sciences du Climat et de l'Environnement, 91198 Gif-sur-Yvette, France

**Abstract** - We measured  $^{228}\text{Ra}_{\text{ex}}/^{226}\text{Ra}_{\text{ex}}$  and  $^{226}\text{Ra}_{\text{ex}}/\text{Ba}_{\text{ex}}$  ratios in suspended and sinking particles collected at the Oceanic Flux Program (OFP) time-series site in the western Sargasso Sea and compared them to seawater ratios to provide information on the origin and transport of barite ( $\text{BaSO}_4$ ) in the water column.

The  $^{228}\text{Ra}_{\text{ex}}/^{226}\text{Ra}_{\text{ex}}$  ratios of the suspended particles down to 2000 m are nearly identical to those of seawater at the same water depth. These ratios are much lower than expected if suspended barite was produced in surface waters and indicates that barite is produced throughout the mesopelagic layer. The  $^{228}\text{Ra}_{\text{ex}}/^{226}\text{Ra}_{\text{ex}}$  activity ratios of sinking particles collected at 1500 m and 3200 m varied mostly between 0.1 to 0.2, which is intermediate between the seawater ratio at these depths ( $< 0.03$ ) and the seawater ratios found in the upper 250 m (0.31-0.42). This suggests that excess Ba (i.e.  $\text{Ba}_{\text{ex}} = \text{Ba}_{\text{total}} - \text{Ba}_{\text{lithogenic}}$ ), considered to be mainly barite, present in the sinking flux is a mixture of crystals formed recently in the upper water column, formed several years earlier in the upper water column, or formed recently in deeper waters. We observe a sizeable temporal variability in the  $^{228}\text{Ra}_{\text{ex}}/^{226}\text{Ra}_{\text{ex}}$  ratios of sinking particles, which indicates temporal variability in the relative proportion of barite crystals originating from surface (with a high  $^{228}\text{Ra}_{\text{ex}}/^{226}\text{Ra}_{\text{ex}}$  ratio) and mesopelagic (with a low  $^{228}\text{Ra}_{\text{ex}}/^{226}\text{Ra}_{\text{ex}}$  ratio) sources. However, we could not discern a clear pattern that would elucidate the factors that control this variability.

The  $^{226}\text{Ra}/\text{Ba}$  ratios measured in seawater are consistent with the value reported from the GEOSECS expeditions (2.3 dpm  $\mu\text{mol}^{-1}$ ) below 500 m depth, but are significantly lower in the upper 500 m. High  $^{226}\text{Ra}_{\text{ex}}/\text{Ba}_{\text{ex}}$  ratios and elevated Sr concentrations in suspended particles from the upper water column suggest preferential uptake of  $^{226}\text{Ra}$  over Ba during formation of  $\text{SrSO}_4$  skeletons by acantharians, which must contribute to barite formation in shallow waters. Deeper in the water column the  $^{226}\text{Ra}_{\text{ex}}/\text{Ba}_{\text{ex}}$  ratios of suspended particles are lower than those of seawater. Since  $^{228}\text{Ra}_{\text{ex}}/^{226}\text{Ra}_{\text{ex}}$  ratios demonstrate that suspended barite at these depths has been produced recently and in situ, their low  $^{226}\text{Ra}_{\text{ex}}/\text{Ba}_{\text{ex}}$  ratios indicate preferential uptake of Ba over Ra in barite formed in mesopelagic water.

Keywords :  $\text{BaSO}_4$ , radium isotopes, particles, acantharians

\* Corresponding author

Tel. + 33 (0)5 61 33 30 03

Fax + 33 (0)5 61 25 32 05

Email : vanbeek@notos.cst.cnes.fr

## 1. INTRODUCTION

Radium isotopes ( $^{228}\text{Ra}$ ,  $T_{1/2}=5.75$  y, and  $^{226}\text{Ra}$ ,  $T_{1/2}=1602$  y) and barium (Ba) have been widely used to study ocean circulation and marine biogeochemical cycling. The global oceanic distribution of these elements and isotopes was first documented during the GEOSECS program (Broecker et al., 1967; Wolgemuth and Broecker, 1970; Bacon and Edmond, 1972; Li et al., 1973; Broecker et al., 1976; Ku and Lin, 1976; Chan et al., 1976; Chung and Craig, 1980; Ku et al., 1980). Water column profiles of  $^{226}\text{Ra}$  and Ba show a similar depletion in surface water and increasing deep water concentrations from the Atlantic to the Pacific Ocean. This similarity between  $^{226}\text{Ra}$  and barium water column profiles was attributed to the nearly identical chemical properties of the two elements (Wolgemuth and Broecker, 1970).  $^{226}\text{Ra}$  and Ba thus show a general linear correlation over much of the water column in the Atlantic, Antarctic and Pacific Oceans, with the result that the  $^{226}\text{Ra}/\text{Ba}$  ratio is fairly constant in the ocean (Li et al., 1973; Chan et al., 1976; Ku et al., 1980; Foster et al., 2004). Based on data from the Atlantic and Pacific Oceans, Chan et al. (1976) estimated this ratio at  $4.6 \text{ nmol } ^{226}\text{Ra}/ \text{mol Ba}$  (i.e.  $2.3 \text{ dpm } \mu\text{mol}^{-1}$ ), similar to the ratios reported in other places of the world (Li et al., 1973; Ku et al., 1980; Foster et al., 2004). In near-bottom waters, however, the correlation breaks down, with  $^{226}\text{Ra}$  activities being higher than those predicted from the radium-barium correlation because of the input of  $^{226}\text{Ra}$  from deep-sea sediments (Chung, 1974; Chan et al., 1976; Chung, 1980; Ku et al., 1980; Rhein et al., 1987). This effect is particularly pronounced in the deep-northeast Pacific (Chan et al., 1974; Chung, 1976).

In contrast to  $^{226}\text{Ra}$ , dissolved  $^{228}\text{Ra}$  activities are highest in the upper water column and decrease rapidly through the permanent pycnocline (Kaufman et al., 1973; Li et al., 1980; Moore, 1987). The high  $^{228}\text{Ra}$  activities in the upper water column and deep waters reflect lateral

transport of  $^{228}\text{Ra}$  that diffused from shelf sediments and release from deep-sea sediments, respectively. The low activities in intermediate waters reflect the slow vertical mixing compared to radioactive decay.

Surface depletion of Ba and  $^{226}\text{Ra}$  results mainly from barite precipitation in the upper water column and release from settling particles (Chow and Goldberg, 1960; Dehairs et al., 1980; Bishop, 1988; Stroobants et al., 1991; Dehairs et al., 1990). Barite precipitation in the upper water column appears to take place within supersaturated microenvironments that result from the decay of organic matter (Chow and Goldberg, 1960; Dehairs et al., 1980; Bishop, 1988; Stroobants et al., 1991; Ganeshram et al., 2003). The correlation of particulate Ba flux and export flux of organic carbon (Dymond et al., 1982; François et al., 1995) has led to the use of barite accumulation rates in deep-sea sediments for paleoproductivity reconstructions (Schmitz, 1987; Gingele and Dahmke, 1994; Paytan et al., 1996a; Nürnberg et al., 1997).

Additionally, it has been proposed that dissolution of celestite ( $\text{SrSO}_4$ ) skeletons made by acantharians and enriched in barium might contribute significantly to barite formation (Bernstein et al., 1987, 1992, 1998; Bernstein and Byrne, 2004). Acantharians are documented as ubiquitous and abundant marine protozoans. Their presence is especially well-documented in the Sargasso Sea (Michaels, 1988; Michaels et al., 1995; Bernstein et al., 1992, 1998). Acantharians are generally concentrated in surface waters and their abundance rapidly decreases below 150 m because celestite rapidly dissolves after the death of the organism (Bishop et al., 1977, 1978; Michaels 1988; Michaels et al., 1995; Bernstein et al., 1992). Bernstein et al. (1992) reported the presence of acantharians as deep as 400 m but specimen became very rare to inexistent in their trap located at 1500 m. These authors also described the presence of large number of cysts and minute  $\text{SrSO}_4$  particles that could be related to the acantharian reproductive cycle. Because acantharians and acantharian-derived particles are enriched in barium and are also expected to

incorporate radium, Bernstein et al.(1992, 1998) suggested that acantharians might play a substantial role in oceanic Ba and Ra cycling.

When barite precipitates, it acquires the  $^{228}\text{Ra}/^{226}\text{Ra}$  ratio of the ambient seawater at the time and depth of formation (Legeleux and Reyss, 1996). Legeleux and Reyss (1996) compared the  $^{228}\text{Ra}/^{226}\text{Ra}$  ratio of sinking particles collected with sediment traps in the tropical northeast Atlantic Ocean to that of seawater. From the sharp decrease in seawater  $^{228}\text{Ra}/^{226}\text{Ra}$  ratio with depth, they argued that the relatively high  $^{228}\text{Ra}/^{226}\text{Ra}$  measured in deep sediment trap material indicated that most of the particulate Ba (presumably barite) is formed in the upper 250 m of the water column. Moore and Dymond (1991) measured the  $^{226}\text{Ra}/\text{Ba}$  ratio in sinking particles collected in the equatorial Pacific and found that particles removed  $^{226}\text{Ra}$  and Ba from waters in the upper water column with a ratio similar to that of seawater. Also observed was a decrease in the  $^{226}\text{Ra}/\text{Ba}$  ratios of particles with depth, which they attributed to the presence of old barite crystals (with low  $^{226}\text{Ra}/\text{Ba}$  ratio due to  $^{226}\text{Ra}$  decay) that were either laterally transported from continental margins or resuspended from the seafloor by deep-sea currents.

The  $^{226}\text{Ra}$  decay in barite accumulated in deep-sea sediments has also been used to estimate Holocene sedimentation rates (Paytan et al., 1996b; van Beek and Reyss, 2001; van Beek et al., 2002; van Beek et al., 2004). Dating of marine carbonate shells has also been attempted (Berkman and Ku, 1998; Staubwasser et al., 2004). The latter method, however, relies on knowing the initial  $^{226}\text{Ra}/\text{Ba}$  ratio incorporated by carbonates, which can be assumed to be 4.6 nmol  $^{226}\text{Ra}/\text{mol Ba}$  or 2.3 dpm  $\mu\text{mol}^{-1}$  (that is, the seawater ratio found to be fairly constant in the oceans; Chan et al., 1976). Both applications require a better understanding of the factors that control i) the seawater Ba and  $^{226}\text{Ra}$  distributions and ii) the incorporation of  $^{226}\text{Ra}$  in particulate phases such as barite or carbonates.

Analysis of radium isotopes in particulate Ba can thus provide information on its origin and flux in the water column and more generally on processes such as advection, resuspension and isopycnal mixing that influence the transport of suspended particles in the ocean. In this study, we measured Ba concentrations,  $^{226}\text{Ra}/\text{Ba}$  and  $^{228}\text{Ra}/^{226}\text{Ra}$  ratios in seawater and in suspended and sinking particles collected at the Oceanic Flux Program (OFP) site in the western Sargasso Sea off Bermuda (31°50'N; 64°10'W; 4500 m water depth) to track barite formation and transport in the water column. To our knowledge, this work reports the first  $^{226}\text{Ra}$  and  $^{228}\text{Ra}$  activities measured in suspended particles. This allowed us to combine seawater data with data from both the sinking and suspended particle pools. Additionally, because previous studies reported abundant acantharian populations in the Sargasso Sea, which might influence the Ba and Ra distributions, Sr contents were analyzed in suspended particles to track the presence of acantharians.

## **2. MATERIAL AND METHODS**

### **2.1. Sample Collection**

The Oceanic Flux Program (OFP) sediment trap time-series mooring (Conte et al., 2001) is located in the northern Sargasso Sea in a transitional region between relatively eutrophic waters to the north and oligotrophic subtropical waters to the south. In addition to the OFP sediment trap time-series, the area is the site of the Bermuda-Atlantic Times Series (BATS, Steinberg et al., 2001) and the Bermuda testbed Mooring (BTM, Dickey et al., 2001).

Seawater samples were collected at the OFP site in May 2002 (from 4<sup>th</sup> to 8<sup>th</sup>) using a CTD equipped with 12 litres-Niskin bottles. Sixty ml samples were collected for dissolved Ba measurements. For Ra isotopes, 50 to 60 litres of seawater were passed through a cartridge filled

with MnO<sub>2</sub>-coated fibres that retain radium isotopes (Moore and Reid, 1973; Moore et al., 1985). The fibres were then ashed (one day at 820°C) and transferred into counting vials for gamma counting.

Suspended particles were collected using McLane large volume in situ pumps (WTS, McLane Labs, Falmouth Ma, USA). Up to 2300 litres were filtered through 142 mm-diameter Versapor filters (acrylic copolymer on a nylon substrate; Pall Corporation), with a pore size of 0.8 µm. Only one depth could not be sampled as planned because the pump did not work (i.e. pump deployed at 3250 m depth).

Sinking particles were collected using Parflux Mark VII sediment traps (McLane Labs, Falmouth MA, USA). Details of OFP sample collection and processing are given in Conte et al. (2001). Sediment trap samples were analyzed from both the 1500 and 3200 m depth traps. Analyses were conducted on archived dried material collected in 1988-1989 and 1999-2000. The integrated period of samples was 58-76 days in 1988-89 and 14-15 days in 1999-2000 (Table 3).

## **2.2. Analytical Methods**

### *2.2.1. Seawater*

Seawater was analysed for barium by isotope dilution using a <sup>135</sup>Ba spike (precision: ± 2 % estimated from replicate analyses), using the ICP/MS facility at Woods Hole Oceanographic Institution (Element, Finnigan). Ra isotopes adsorbed on MnO<sub>2</sub> ash were counted at the underground laboratory of Modane (French Alps). High-efficiency, low-background, well-type germanium detectors (215 cm<sup>3</sup>, 430 cm<sup>3</sup> and 950 cm<sup>3</sup>) were used (Reyss et al., 1995). <sup>226</sup>Ra activities were determined using the <sup>214</sup>Pb (295 keV and 352 keV) and <sup>214</sup>Bi (609 keV) peaks. <sup>228</sup>Ra activities were determined using the 338 keV, 911 keV and 969 keV peaks of <sup>228</sup>Ac.

Counting time for each sample ranges from 2 to 5 days. Uncertainties reported for  $^{226}\text{Ra}$  and  $^{228}\text{Ra}$  activities are errors due to counting statistics.

### 2.2.2. Suspended Particles

Ra isotopes were first measured on intact filters by gamma counting using the same method used for the  $\text{MnO}_2$  ashed samples. The Versapor filters were subsequently dissolved in a Teflon beaker with a mixture of  $\text{HNO}_3$  (ultrapure acid),  $\text{HF}$  (ultrapure acid), and  $\text{HClO}_4$  (pure acid) placed on a hot plate. Barium and strontium concentrations were measured at LEGOS by ICP-MS using a Elan 6000 Perkin Elmer (reproducibility of the method estimated at  $\pm 4\%$ ) using external standards. Na and Ca were analysed by atomic spectrophotometry at OMP, Toulouse.  $^{232}\text{Th}$  was measured by ICP/MS (VG PlasmaQuad II) at the Scottish Universities Research and Reactor Centre, East Kilbride, also using external standards (reproducibility of the method estimated at  $\pm 4\%$ ).

As particulate Ba and Ra are mainly associated with barite and lithogenic material in the water column, we calculated excess Ba concentration ( $\text{Ba}_{\text{ex}}$ ) and excess Ra activities ( $^{226}\text{Ra}_{\text{ex}}$  and  $^{228}\text{Ra}_{\text{ex}}$ ) in suspended particles that refer to the Ba and Ra associated with barite. Ba and Ra concentrations were corrected for lithogenic fraction using the following equations:

$$\text{Ba}_{\text{ex}} = \text{Ba}_{\text{total}} - (^{232}\text{Th} \times [\text{Ba}/^{232}\text{Th}]_{\text{upper crust}}) \quad (1)$$

$$^{226}\text{Ra}_{\text{ex}} = ^{226}\text{Ra}_{\text{total}} - (^{238}\text{U} \cdot ^{226}\text{Ra}) \quad (2)$$

$$^{228}\text{Ra}_{\text{ex}} = ^{228}\text{Ra}_{\text{total}} - (^{232}\text{Th} \cdot ^{228}\text{Ra}) \quad (3)$$

Where  $\text{Ba}_{\text{total}}$ ,  $^{226}\text{Ra}_{\text{total}}$  and  $^{228}\text{Ra}_{\text{total}}$  refer to the total concentrations or activities;  $[\text{Ba}/^{232}\text{Th}]_{\text{upper crust}}$  is the mean ratio (ppm/ppm) for the upper crust (51.4; Taylor and McLennan,

1985); ( $^{238}\text{U}$ - $^{226}\text{Ra}$ ) and ( $^{232}\text{Th}$ - $^{228}\text{Ra}$ ) refer to the  $^{226}\text{Ra}$  and  $^{228}\text{Ra}$  activities in radioactive equilibrium with lithogenic  $^{238}\text{U}$  and  $^{232}\text{Th}$ , respectively. The  $^{232}\text{Th}$  activities measured were assumed to be entirely lithogenic. The lithogenic  $^{238}\text{U}$  activities were estimated from the  $^{232}\text{Th}$  activities, using the upper continental crust  $^{238}\text{U}/^{232}\text{Th}$  ratio of 0.8 (dpm/dpm ; Taylor and McLennan, 1985). While oceanic particles may often contain an authigenic U fraction, this is assumed to be too recent to be associated with significant  $^{226}\text{Ra}$  ingrowth. Errors on the excess concentrations were obtained by propagating the errors of each elemental concentrations (Ba,  $^{226}\text{Ra}$ ,  $^{228}\text{Ra}$  as well as  $^{232}\text{Th}$ ). This does not include error associated with the crustal ratios (Taylor and McLennan, 1985) used in the calculations.

As  $\text{SrSO}_4$  is the major structural component of acantharians, we measured Sr concentrations in particles to track the presence of acantharians. Sr in particles may also be associated with carbonates. Following Bishop (1977), we estimated non-carbonate Sr concentrations that will be related to acantharians :

$$\text{non-carbonate Sr} = \text{Sr}_{\text{total}} - \text{Sr}_{\text{carbonate}} \quad (4)$$

First, we corrected the Sr concentrations determined from filters collected with in situ pumps for the sea-salt contribution by analysing the Na content and considering a Sr/Na ratio in seawater of 0.00019 (mol/mol). The Sr content of the carbonate fraction was calculated assuming that carbonates contained 0.17 mole percent Sr (Bishop et al., 1977). Carbonate content was estimated from the Ca concentration corrected for i) the sea-salt contribution (using a Ca/Na ratio of 0.0219 mol/mol in seawater) and ii) the lithogenic Ca phase using a crustal Ca/Th ratio (ppm/ppm) of 2804 (Taylor and McLennan, 1985). Uncertainty on particulate Sr concentrations is estimated at 10 % due to the different corrections (propagation of errors). This does not include error associated with the crustal ratios used in the calculations. Correction for the Sr associated with

sea-salt is ca. 35 % for most samples but was higher for samples above 200 m (ca. 50 %) and reached 83 % for the 20 m pump sample.

### *2.2.3. Sinking Particles*

Sediment trap samples were first analyzed for Ra isotopes by gamma counting at Modane. Ba and  $^{232}\text{Th}$  were then measured by instrumental neutron activation for samples collected in 1988-1989 (LSCE, Gif-sur-Yvette) and ICP/MS (Elan 6000 Perkin Elmer; OMP, Toulouse) for samples collected in 1999-2000. For neutron activation analysis, samples were placed 5 minutes in the Osiris nuclear reactor (Laboratoire Pierre Süe, Saclay, France) and measured for their radioactivity using the germanium detectors located in Gif-sur-Yvette, France (precision:  $\pm 5\%$  estimated from replicate analyses of standards). For ICP/MS analysis, samples were digested in a microwave using a mixture of HF and  $\text{HNO}_3$  prior to analysis (precision:  $\pm 3\%$  estimated from replicate analyses of standards).

Excess Ba,  $^{226}\text{Ra}$  and  $^{228}\text{Ra}$  were calculated as explained in the suspended particles section.  $^{228}\text{Ra}_{\text{ex}}$  activities of sinking particles were also corrected for radioactive decay since the time of sampling (denoted  $^{228}\text{Ra}_{\text{ex}}^{\circ}$  in Tab. 3). In contrast,  $^{228}\text{Ra}$  activities of suspended particles and seawater samples were not decay-corrected because gamma counting of the samples was performed within the 5 months following sample collection.

## **3. RESULTS**

### **3.1 Hydrology**

The vertical structure and circulation of water masses in the region has been previously reviewed by Talley (1996), Joyce and Robbins (1996) and references therein. A CTD profile collected on the OFP cruise and discrete nutrient data collected on an earlier BATS cruise provided information on vertical structure of water masses that was pertinent to the samples collected (Fig. 1). Below a 30 m surface mixed layer, variable salinity indicated a complex water mass structure within and below the seasonal thermocline, including a distinctive lense of fresher water lying between 160-180 m. Subtropical Mode Water (“18°C water”), which outcrops in the northern Sargasso Sea just south of the Gulf Stream, was found between 275-400 m. The depth of the O<sub>2</sub> minimum was 890 m, just above the maxima in AOU, NO<sub>3</sub> and PO<sub>4</sub>. An influence of westward spreading Mediterranean water is suggested by positive excursions in salinity and negative excursions in O<sub>2</sub> and PO<sub>4</sub> at depths between 980-1200 m and 1300-1470 m. The core of the southward flowing Labrador Sea Water (LSW), a high oxygen and low salinity water mass of sigma theta 27.78, was centered at 1650 m, above the North Atlantic Deep Water. Antarctic Bottom Water (AABW), identified by a potential T<1.90°C and high nutrients, was present below 3800 m.

## **3.2 Elemental Concentrations and Ratios**

### *3.2.1 Seawater*

Barium, <sup>226</sup>Ra and <sup>228</sup>Ra profiles (Fig. 2; Tab.1) are similar to those reported earlier for the Atlantic Ocean (Broecker et al., 1967; Wolgemuth and Broecker, 1970; Kaufman et al., 1973; Broecker et al., 1976; Chan et al., 1976; Chan et al., 1977; Moore et al., 1985; Kim et al., 2003). Barium concentrations and <sup>226</sup>Ra activities in seawater increase with depth, reflecting uptake during particle formation in shallow waters and subsequent release to the deep water from

settling particles. Ba and  $^{226}\text{Ra}$  contents are relatively constant in the upper 400 m (ca.  $44.4 \mu\text{mol l}^{-1}$  Ba; ca.  $8.6 \text{ dpm}/100 \text{ kg } ^{226}\text{Ra}$ ) and increase with increasing water depth.  $^{226}\text{Ra}$  activities increase in two steps to a maximum of  $17.5 \text{ dpm}/100 \text{ kg}$  near the seafloor. The steep increase in Ba concentrations and  $^{226}\text{Ra}$  activities below 3700 m can be associated with Antarctic Bottom Water which are enriched in Ba and  $^{226}\text{Ra}$  (Broecker et al., 1976; Li et al., 1973; Jacquet et al., 2004).

The  $^{228}\text{Ra}$  activity profile at the OFP site displays a strong vertical gradient from surface to intermediate waters.  $^{228}\text{Ra}$  activities increase again close to the bottom due to diffusion from deep-sea sediment. The dissolved  $^{228}\text{Ra}/^{226}\text{Ra}$  seawater profile shows a similarly strong vertical gradient in the upper water column (Fig. 4). Our data agree with those of Kim et al. (2003) who reported  $^{228}\text{Ra}/^{226}\text{Ra}$  ratios from the upper 600 m in the same area.

The dissolved  $^{226}\text{Ra}/\text{Ba}$  ratios below 500 m are close to  $2.3 \text{ dpm } \mu\text{mol}^{-1}$  (that is, the value reported by Chan et al., 1976), which can be considered as a reference value, but we find significantly lower values in the upper 500 m of the water column, above the main thermocline (Fig. 5).

### 3.2.2 Suspended Particles (In Situ Pumps)

3.2.2.1 *Barium*. Particulate barium concentrations are higher in the upper 1500 m and especially in the upper 500 m (Fig. 3). They are low at 20 m but peak at 70 m ( $0.24 \text{ nmol kg}^{-1}$ ) and 300 m ( $0.18 \text{ nmol kg}^{-1}$ ). These concentrations are in the same range as the values reported by Bishop (1988) in the Sargasso Sea. They are 2 orders of magnitude lower than the Ba concentrations in seawater. Barite is generally considered the main carrier (Dehairs et al., 1980; Bishop, 1988; Dehairs et al., 1990, 1991), with a smaller contribution from lithogenic material. To correct for

the latter, excess Ba concentrations ( $Ba_{ex}$ ) were calculated by subtracting lithogenic Ba estimated from particulate  $^{232}Th$  concentrations. The lithogenic fraction is relatively small and constant throughout the water column but increases sharply below ca. 4000 m, reflecting the presence of a bottom nepheloid layer (Fig. 3; Tab. 2). Sherrell and Boyle (1992) reported a similar increase in particulate Al and Fe concentrations towards the bottom in the water column near Bermuda. Using their Al data and a Ba/Al ratio of 0.0075, we obtain lithogenic Ba concentrations which are in good agreement with our estimates. The lithogenic correction is small in the upper 1500 m and  $Ba_{ex}$  concentrations remain high (Fig.3). In contrast, the Ba content of suspended particles collected in deep waters is dominated by lithogenic Ba, and no  $Ba_{ex}$  could be found in the upper nepheloid layer, indicating a substantial decrease in suspended barite concentration with depth. Note that the lithogenic Ba deduced from  $^{232}Th$  concentrations is higher than the Ba content measured in sample collected at 4000 m. Uncertainty associated with the crustal Ba/Th ratio used to calculate the lithogenic Ba may explain such pattern.

3.2.2.2 *Radium isotopes.*  $^{226}\text{Ra}$  activities in suspended particles are highest in surface waters (0.09 dpm/ 100 kg, ie. two orders of magnitude lower than the  $^{226}\text{Ra}$  activity in seawater) and decrease with depth, with a secondary peak at 300 m (Fig.3). The excess  $^{226}\text{Ra}$  profile is similar to that of excess Ba (Fig.3). Suspended  $^{226}\text{Ra}_{\text{ex}}$  activities are highest in the upper 500 m, where the lowest dissolved  $^{226}\text{Ra}$  activities are found (Fig. 1), and decrease with depth before increasing slightly towards the seafloor. Particulate  $^{228}\text{Ra}$  activities are also highest towards the surface and decrease rapidly to very low values in mid water. Very little or no excess  $^{228}\text{Ra}$  activity remains in suspended particles below 1000 m.  $^{228}\text{Ra}_{\text{ex}}/^{226}\text{Ra}_{\text{ex}}$  activity ratios (Fig. 4 and Tab. 2) display a similar profile. For sample collected at 4000 m, note that the  $^{232}\text{Th}$  activity is higher than that of  $^{228}\text{Ra}$ .

3.2.2.3  *$^{226}\text{Ra}/\text{Ba}$  ratios and Sr contents.*  $^{226}\text{Ra}_{\text{ex}}/\text{Ba}_{\text{ex}}$  ratios in suspended particles collected in the upper 170 m are higher than  $2.3 \text{ dpm } \mu\text{mol}^{-1}$ , reaching a maximum ( $3.8 \text{ dpm } \mu\text{mol}^{-1}$ ) at 120 m depth (Fig.5). Such values are higher than the maximum value reported by Moore and Dymond (1991) when analyzing sediment trap material from the Pacific Ocean. Below 120 m,  $^{226}\text{Ra}_{\text{ex}}/\text{Ba}_{\text{ex}}$  ratios exhibit a constant decrease with increasing depth. From 300 m to 700 m,  $^{226}\text{Ra}_{\text{ex}}/\text{Ba}_{\text{ex}}$  ratios are close to the value of  $2.3 \text{ dpm } \mu\text{mol}^{-1}$ . Below 1000 m,  $^{226}\text{Ra}_{\text{ex}}/\text{Ba}_{\text{ex}}$  ratios are lower, with values as low as  $1.33 \text{ dpm } \mu\text{mol}^{-1}$  at 2380 m.

Sr contents in suspended particles are also high in the upper 150 m (Fig. 5). Sr values (total Sr corrected for sea-salt as well as non-carbonate-Sr) are similar to values reported by Bishop et al. (1977, 1978) who analyzed suspended particles also collected using in situ pumps in the Atlantic Ocean. Maximum non-carbonate-Sr concentrations are found at 120 m. Below this depth, non-carbonate Sr concentrations decrease with increasing water depth down to ca. 1500 m. Deeper in the water column, Sr contents display constant values.

### 3.2.3 Sinking Particles (Sediment Traps)

3.2.3.1  $^{228}\text{Ra}_{\text{ex}}/^{226}\text{Ra}_{\text{ex}}$  ratio. The range of  $^{228}\text{Ra}_{\text{ex}}/^{226}\text{Ra}_{\text{ex}}$  ratios found in sinking particles collected during the two different periods is very similar (Fig. 6, Tab. 3). In most cases, the ratios range between 0.1 to 0.2, with significant variability. Note that for several samples from the deeper sediment trap, no significant excess  $^{228}\text{Ra}$  activities could be found. In most cases the ratio found in the deep sediment trap at 3200 m is lower than the ratio found at 1500 m.

3.2.3.2  $^{226}\text{Ra}_{\text{ex}}/\text{Ba}_{\text{ex}}$  ratio.  $^{226}\text{Ra}_{\text{ex}}/\text{Ba}_{\text{ex}}$  ratios also display significant variability with time and water depth (0.53-4.09 dpm  $\mu\text{mol}^{-1}$ , Fig. 7). In most cases, the  $^{226}\text{Ra}_{\text{ex}}/\text{Ba}_{\text{ex}}$  ratio found at 3200 m is lower than the ratio found at 1500 m, with, however, two samples showing the opposite trend (i.e. february-april 1989 and june 2000). Two samples collected at 1500 m in 1988 (i.e. march-may and july-september) display  $^{226}\text{Ra}_{\text{ex}}/\text{Ba}_{\text{ex}}$  ratios much higher than the seawater ratio ( $> 3.5$  dpm  $\mu\text{mol}^{-1}$ ). Sediment trap material from the Pacific Ocean analyzed by Moore and Dymond (1991) did not exhibit such high values.  $^{226}\text{Ra}_{\text{ex}}/\text{Ba}_{\text{ex}}$  ratios found in samples collected in 1999-2000 were all  $< 2.1$  dpm  $\mu\text{mol}^{-1}$ , with most of the samples displaying ratios lower than the seawater ratios reported in this study ( $< 1.5$  dpm  $\mu\text{mol}^{-1}$ ).

## 4. DISCUSSION

### 4.1. $^{228}\text{Ra}_{\text{ex}}/^{226}\text{Ra}_{\text{ex}}$ Ratios

Previous studies have suggested that barite precipitation takes mainly place in the upper 500 m of the water column (Chow and Goldberg, 1960; Dehairs et al., 1980; Bishop et al., 1988; Dehairs et al., 1990, 1991, 1992; Legeleux and Reyss, 1996), which could account for the higher

particulate excess Ba and  $^{226}\text{Ra}$  concentrations found in the upper 500 m at the OFP site. Suspended barite found deeper in the water column could have been produced in situ (that is, at the depth of sample collection) or could have been released from aggregates settling from shallower depth. When studying suspended particles in the Sargasso Sea, Bishop (1988) concluded that barite crystals formed in the  $>53\ \mu\text{m}$  particle size fractions in near-surface waters and were released into the 1-53  $\mu\text{m}$  fraction at depths below the euphotic zone (at 200-300 m). Such release could occur also deeper in the water column. The decreasing trend in  $\text{Ba}_{\text{ex}}$  and  $^{226}\text{Ra}_{\text{ex}}$  particulate concentration with depth (Fig. 3) could thus reflect a decrease in supply of fine barite crystals by breakdown of settling particles which is expected to be more intensive in the upper 500 m. Once released from the supersaturated microenvironments in which they presumably formed, barite crystals would be subjected to dissolution in undersaturated waters (Church and Wolgemuth, 1972; Monnin et al., 1999; Rushdi et al., 2000). Thus, the decrease in particulate  $\text{Ba}_{\text{ex}}$  and  $^{226}\text{Ra}_{\text{ex}}$  with depth could also be partly driven by gradual dissolution during settling. In addition, barite may also precipitate in deep water. The decreasing trend of  $\text{Ba}_{\text{ex}}$  profile could thus reflect a decrease in the rate at which barite is produced in situ. With its strong gradient in the upper water column, the  $^{228}\text{Ra}_{\text{ex}}/^{226}\text{Ra}_{\text{ex}}$  of suspended and sinking particles can provide some clarification on the relative importance of these various processes.

#### 4.1.1 $^{228}\text{Ra}_{\text{ex}}/^{226}\text{Ra}_{\text{ex}}$ Ratio in Suspended Particles

When precipitating, barite incorporates radium isotopes from seawater at the depth of formation. Because the  $^{228}\text{Ra}/^{226}\text{Ra}$  ratio in seawater displays a strong vertical gradient (Fig. 4), the  $^{228}\text{Ra}/^{226}\text{Ra}$  ratio of barite can be used to constrain the depth range of barite formation

(Legeleux and Reyss, 1996). Barite forming in the upper water column should have higher  $^{228}\text{Ra}/^{226}\text{Ra}$  ratios than barite produced in deeper water.

In the upper 500 m, the  $^{228}\text{Ra}_{\text{ex}}/^{226}\text{Ra}_{\text{ex}}$  ratios in suspended particles are high (0.22-0.35 dpm/ 100 kg) and are close to the seawater ratio given for the same water depth (Fig. 4). This pattern agrees with the idea that barite crystals form in the upper water column, as was reported by previous studies (Dehairs et al., 1980; Bishop, 1988; Dehairs et al., 1990, 1991; Legeleux and Reyss, 1996) and as was suggested by the higher excess Ba concentrations found in this work in the upper 500 m. Deeper in the water column, the  $^{228}\text{Ra}_{\text{ex}}/^{226}\text{Ra}_{\text{ex}}$  of suspended particles rapidly decreases to zero below 1000 m.

Suspended particles settle to the seafloor via cycles of aggregation and disaggregation. They sink rapidly ( $> 100$  m/ day) when incorporated into large sinking particles, and very slowly when released by disaggregation. Their mean sinking rates (300 – 1000 m/ y) have been estimated from measurements of the  $^{230}\text{Th}$  in fine suspended particles (Krishnaswami et al., 1981; Bacon and Anderson, 1982; Bacon et al., 1985). If all the suspended  $\text{Ba}_{\text{ex}}$  found in deep water were produced in surface water with a  $^{228}\text{Ra}/^{226}\text{Ra}$  of 0.38, we could predict their  $^{228}\text{Ra}_{\text{ex}}/^{226}\text{Ra}_{\text{ex}}$  depth profile for a given sinking rate  $S$  (Fig. 8):

$$[^{228}\text{Ra}_{\text{ex}}/^{226}\text{Ra}_{\text{ex}}]_z = [^{228}\text{Ra}_{\text{ex}}/^{226}\text{Ra}_{\text{ex}}]_0 \exp(-\lambda_{228} z / S) \quad (5)$$

We also plotted the predicted  $^{228}\text{Ra}_{\text{ex}}/^{226}\text{Ra}_{\text{ex}}$  depth profile of suspended particles considering that suspended  $\text{Ba}_{\text{ex}}$  was produced in subsurface ( $\sim 250$  m) with a ratio of 0.30. This is because it has often been proposed that barite predominantly formed in subsurface, in the vicinity of the oxygen minimum (Dehairs et al., 1980, 1990; Stroobants et al., 1991; Dehairs et al., 1992). Fitting the particulate  $^{228}\text{Ra}_{\text{ex}}/^{226}\text{Ra}_{\text{ex}}$  data requires a mean sinking velocity of 40 m/ y, which is well below the range of values estimated from particulate  $^{230}\text{Th}$ . This observation implies that  $\text{Ba}_{\text{ex}}$  must also be produced in deeper water with lower initial  $^{228}\text{Ra}_{\text{ex}}/^{226}\text{Ra}_{\text{ex}}$  ratios. In addition, since the

$^{228}\text{Ra}_{\text{ex}}/^{226}\text{Ra}_{\text{ex}}$  of suspended particles is very close (within error bars) to the seawater ratios (Fig. 4), our data suggest very little contribution from aged barite crystals originating from the surface.

We can predict the  $^{228}\text{Ra}_{\text{ex}}$  activity profile of suspended particles if all  $\text{Ba}_{\text{ex}}$  was produced in situ (i.e. at the depth of sample collection) from the measured  $^{226}\text{Ra}_{\text{ex}}$  activities and the  $^{228}\text{Ra}/^{226}\text{Ra}$  ratios of seawater (Fig. 8) :

$$\text{Predicted}[^{228}\text{Ra}_{\text{ex}}]_z = \text{Measured}[^{226}\text{Ra}_{\text{ex}}]_z \times \text{Seawater}(^{228}\text{Ra}/^{226}\text{Ra})_z \quad (6)$$

Similarly, we can predict  $^{228}\text{Ra}_{\text{ex}}$  activity profile if all  $\text{Ba}_{\text{ex}}$  was produced in surface water or subsurface and sinking at rates  $S$  ranging from 300 to 1000 m/ y.

$$\text{Predicted}[^{228}\text{Ra}_{\text{ex}}]_z = \text{Measured}[^{226}\text{Ra}_{\text{ex}}]_z \times \text{Seawater}(^{228}\text{Ra}/^{226}\text{Ra})_0 \times \text{EXP}(\lambda_{228} z / S) \quad (7)$$

$\text{Seawater}(^{228}\text{Ra}/^{226}\text{Ra})_0$  was considered to be 0.38 for surface water and 0.30 for subsurface waters.

The predictions based on in situ production fall within the error bars of the data (Fig. 8), confirming that most of the  $\text{Ba}_{\text{ex}}$  in suspension at depth between 450 m and 2380 m is produced in situ. At 4000 m and below, within the nepheloid layer, all suspended Ba can be accounted for by lithogenic material (fig. 3). These samples appear to be significantly depleted in  $^{228}\text{Ra}$  (i.e.  $^{228}\text{Ra}$  activity is lower than  $^{232}\text{Th}$  activity in the same samples), suggesting rapid loss of  $^{228}\text{Ra}$  from resuspended sediment to the water column.

Lateral transport of old sediment resuspended from continental margins to the ocean interior, as suggested by Moore and Dymond (1991), could also explain the low  $^{228}\text{Ra}_{\text{ex}}/^{226}\text{Ra}_{\text{ex}}$  of suspended particles, but such lateral input would also result in higher suspended  $^{232}\text{Th}$  concentration. The latter is relatively constant in the upper 2380 m, showing a significant increase only close to the bottom (Fig. 3; Tab. 2). The low  $^{228}\text{Ra}_{\text{ex}}/^{226}\text{Ra}_{\text{ex}}$  ratios observed between 500 m and 2000 m, therefore, are unlikely to be explained by the lateral transport of particles resuspended at the continental margins.

#### 4.1.2 $^{228}\text{Ra}_{\text{ex}}/^{226}\text{Ra}_{\text{ex}}$ Ratio in Sinking Particles

In most cases, the  $^{228}\text{Ra}_{\text{ex}}/^{226}\text{Ra}_{\text{ex}}$  ratios found in sinking particles at 1500 m and 3200 m are intermediate between that of barite (or particulate  $\text{Ba}_{\text{ex}}$ ) originating from surface or subsurface waters (0.23-0.35) and those formed in deeper water ( $< 0.1$ ; Fig. 6). These intermediate values suggest that a significant fraction of the barite intercepted by the sediment traps originates from the upper water column, as suggested by Legeleux and Reyss (1996), but with equally significant contributions from deeper waters. Considering that there is little evidence of barite release from disaggregation of large particles below 500 m (which would increase  $^{228}\text{Ra}_{\text{ex}}/^{226}\text{Ra}_{\text{ex}}$  ratios of suspended particles to values higher than seawater ratios), it would appear that exchange of  $\text{Ba}_{\text{ex}}$  between the two pools of particles occurs mainly in one direction, i.e. large sinking particles entrain barite produced in deeper water but release little barite to seawater during settling. This suggests that the increase in seawater concentration in Ba and  $^{226}\text{Ra}$  concentration is mainly due to vertical diffusion after dissolution on the seafloor, since dissolution of barite during the short residence time of large particles in the water column is unlikely to be significant.

There is a relatively large temporal and depth variability in the  $^{228}\text{Ra}_{\text{ex}}/^{226}\text{Ra}_{\text{ex}}$  ratios of the sinking particles. Legeleux and Reyss (1996) also reported significant fluctuations with time and water depth in the  $^{228}\text{Ra}_{\text{ex}}/^{226}\text{Ra}_{\text{ex}}$  ratio of sinking particles collected in the tropical northeast Atlantic (ratios ranging from 0.09 to 0.25 at the oligotrophic site and from 0.09 to 0.30 at the mesotrophic site). Such variability suggests significant temporal variations in the relative proportion of barite originating from surface and intermediate waters, but no pattern could be distinguished which would provide insight into what controls this variability. Mass fluxes and  $\text{Ba}_{\text{ex}}$  fluxes display large variations throughout the year (Tab. 3; Conte et al., 2001), but no

significant correlation could be identified between the  $^{228}\text{Ra}_{\text{ex}}/^{226}\text{Ra}_{\text{ex}}$  ratio of sinking particles and any of the downward fluxes (total, organic carbon, silica, carbonates,  $\text{Ba}_{\text{ex}}$ ). This may in part be due to the large uncertainties in the  $^{228}\text{Ra}$  measurements.

On occasion,  $^{228}\text{Ra}_{\text{ex}}$  activity of settling particles drops below detection limits. In particular, this was observed in the sample collected in winter 1988-1989 and in three of the four samples collected during brief (two weeks) periods in 2000 (Table 3; Fig. 6). In such instances, the intercepted  $\text{Ba}_{\text{ex}}$  could only originate from water deeper than 1000 m, with very little contribution of  $\text{Ba}_{\text{ex}}$  from surface/ subsurface waters. Similarly, the addition of barite crystals precipitated below 1500 m to the downward flux could explain the decrease in the  $^{228}\text{Ra}_{\text{ex}}/^{226}\text{Ra}_{\text{ex}}$  ratio of sinking particles often observed between 1500 m and 3200 m.

#### **4.2. $^{226}\text{Ra}_{\text{ex}}/\text{Ba}_{\text{ex}}$ Ratios**

The study of  $^{226}\text{Ra}_{\text{ex}}/\text{Ba}_{\text{ex}}$  ratios and Sr contents can be used to reinforce our deductions based on  $^{228}\text{Ra}/^{226}\text{Ra}$  data and to provide additional information on the possible role of acantharians in barite formation (Bernstein et al., 1987, 1992, 1998).

##### *4.2.1 Seawater*

Earlier studies have indicated that the dissolved  $^{226}\text{Ra}/\text{Ba}$  ratios in open ocean waters is generally uniform ( $2.3 \text{ dpm } \mu\text{mol}^{-1}$ ; Chan et al., 1976; Foster et al., 2004). The dissolved  $^{226}\text{Ra}/\text{Ba}$  ratios below 500 m agree with this observation, but we find significantly lower values in the upper 500 m of the water column, above the main thermocline (Fig. 5). Similar  $^{226}\text{Ra}/\text{Ba}$  profiles have been found at (old) Hale Aloha station off Hawaii and Station K3 in the North-West Pacific

(van Beek et al., unpublished data), indicating that this is not a feature unique to the OFP site, and suggesting preferential uptake of Ra over Ba in the upper water column. At similar depths, salinity-normalized Sr concentrations in the Sargasso Sea reported small variations but not clear depletion in surface water which could indicate acantharians production (Mackenzie, 1964; Bernstein et al., 1992, 1998).

#### 4.2.2 *Suspended Particles*

In the upper 500 m, fractionation during the formation of suspended particulate Ba is corroborated by the high  $^{226}\text{Ra}_{\text{ex}}/\text{Ba}_{\text{ex}}$  ratios of suspended particles compared to seawater at the same depth (Fig. 5). A depth-by-depth correlation between seawater and suspended particles ratios is not warranted because of the different integration times inherent in the data sets: the seawater ratio reflects a longer-term integration whereas the ratio in suspended particles reflects a “snapshot” view. Nonetheless,  $^{226}\text{Ra}_{\text{ex}}/\text{Ba}_{\text{ex}}$  ratios are clearly higher than  $2.3 \text{ dpm } \mu\text{mol}^{-1}$  in suspended particles collected in the upper 170 m, reaching a maximum ( $3.8 \text{ dpm } \mu\text{mol}^{-1}$ ) at 120 m depth. At the same water depth, a maximum in the non-carbonate-Sr contents is observed (Fig. 5).

To a first approximation, suspended  $\text{Ba}_{\text{ex}}$  was attributed to barite (Dehairs et al., 1980; Bishop, 1988; Dehairs et al., 1990; Stroobants et al., 1991). Bernstein et al. (1992, 1998), however, suggested that acantharian skeletons made of celestite ( $\text{SrSO}_4$ ) could play a significant role in the Ba and Ra cycle. Michaels (1988), Michaels et al. (1995) and Bernstein et al. (1992, 1998) reported the presence of abundant acantharian population in the Sargasso Sea. In the present study, we relate the high non-carbonate Sr concentrations in surface waters to acantharian skeletons. Our Sr data agree with the view that acantharians are generally concentrated in surface

waters and that their abundance rapidly decreases below 150 m because celestite rapidly dissolves after the death of the organism (Bishop et al., 1977, 1978; Michaels 1988; Michaels et al., 1995; Bernstein et al., 1992).

The highest  $^{226}\text{Ra}_{\text{ex}}/\text{Ba}_{\text{ex}}$  ratio reported at 120 m that corresponds to the maximum in the non-carbonate Sr is likely to be associated with acantharian celestite (Fig. 5). Chemical analogues of strontium, both barium and radium are incorporated into celestite. Based on the solubility products of Ra, Ba and Sr sulfate at 20°C and zero ionic strength, Bernstein et al. (1998) predicted radium enrichments in celestite. The relatively high  $^{226}\text{Ra}_{\text{ex}}/\text{Ba}_{\text{ex}}$  ratios and Sr contents in the suspended particles from surface waters therefore likely indicate the presence of acantharians, and their gradual decrease with depth must reflect the gradual dissolution of celestite.

In the absence of acantharians below 500 m in suspended particles,  $\text{Ba}_{\text{ex}}$  concentrations can be more confidently attributed to barite. In these deeper waters, the  $^{226}\text{Ra}_{\text{ex}}/\text{Ba}_{\text{ex}}$  ratios of suspended particle are lower than those of seawater (Fig. 5) and drop below  $2.3 \text{ dpm } \mu\text{mol}^{-1}$ , reaching zero at 4000 m before increasing sharply near the seafloor. Moore and Dymond (1991) also found  $^{226}\text{Ra}_{\text{ex}}/\text{Ba}_{\text{ex}}$  ratios lower than  $2.3 \text{ dpm } \mu\text{mol}^{-1}$  in sinking particles from deep Pacific water, which they attributed to presence of old barite crystals (with a low  $^{226}\text{Ra}/\text{Ba}$  ratio) from resuspended margin or deep-sea sediments. Considering the low  $^{228}\text{Ra}_{\text{ex}}/^{226}\text{Ra}_{\text{ex}}$  and  $^{232}\text{Th}$  activities in the suspended particles at OFP, we concluded that barite formed in situ and were not laterally transported. Particulate ratio lower than seawater ratio would imply a preferential uptake of Ba over Ra during barite precipitation. In the upper 500 m, a similar fractionation would occur during barite precipitation, but this process would occur in microenvironments enriched in  $^{226}\text{Ra}$  by the dissolution of celestite, thereby raising the  $^{226}\text{Ra}_{\text{ex}}/\text{Ba}_{\text{ex}}$  ratio of particulate Ba (or barite) to values equal or higher to that of ambient seawater. In the nepheloid layer,  $\text{Ba}_{\text{ex}}$ ,  $\text{Ra}_{\text{ex}}$  and  $\text{Sr}_{\text{ex}}$  are

small compared to their lithogenic fractions and uncertainties in the lithogenic corrections prevent us to use the excess ratios in a meaningful way.

#### 4.2.3 Sinking Particles

As for  $^{228}\text{Ra}_{\text{ex}}/^{226}\text{Ra}_{\text{ex}}$ , the  $^{226}\text{Ra}_{\text{ex}}/\text{Ba}_{\text{ex}}$  ratios of sinking particles are intermediate between the ratios measured in shallow and deeper water, confirming the mixed origin of barite or  $\text{Ba}_{\text{ex}}$  intercepted by sediment traps.  $^{226}\text{Ra}_{\text{ex}}/\text{Ba}_{\text{ex}}$  ratios also display significant variability with time and water depth (0.53-4.09 dpm  $\mu\text{mol}^{-1}$ ). With smaller error bars, we can better distinguish the origin of  $\text{Ba}_{\text{ex}}$  in different seasons and years. During the 1988-1989 collection period, the  $\text{Ba}_{\text{ex}}$  intercepted at 1500 m clearly had a predominantly shallow signature (high  $^{226}\text{Ra}_{\text{ex}}/\text{Ba}_{\text{ex}}$ ) during Spring and Summer, which is not inconsistent with the  $^{228}\text{Ra}_{\text{ex}}/^{226}\text{Ra}_{\text{ex}}$  ratios of the same samples when considering the error bars on the latter. On the other hand, the winter samples had a predominantly deep signature. It is not possible, however, to tell from this study whether the two highest  $^{226}\text{Ra}_{\text{ex}}/\text{Ba}_{\text{ex}}$  values  $> 3.5$  dpm  $\mu\text{mol}^{-1}$  are associated with i) barite crystals enriched in  $^{226}\text{Ra}$  potentially deriving from the dissolution of acantharians or ii) acantharian specimens and/or acantharian-derived particles. We note that the highest  $^{226}\text{Ra}_{\text{ex}}/\text{Ba}_{\text{ex}}$  values are not associated with the highest Sr flux intercepted by the sediment traps (data not shown), as would be expected if the high ratios are associated with acantharian specimen. In addition, observations of Bernstein et al.(1992) in the Sargasso Sea concluded that acantharian specimen were rare to non-existent at 1500 m depth. However, this is non conclusive.

In the deep trap, the  $^{226}\text{Ra}_{\text{ex}}/\text{Ba}_{\text{ex}}$  ratios can more confidently be associated with barite as acantharians are not recovered at such depth (Bernstein et al., 1992). At 3200 m, the Spring and Summer samples had lower ratios than at 1500 m, suggesting addition of barite produced below

1500 m to the vertical flux. During the 1999-2000 collection period, the ratio of most sediment trap samples suggest a predominantly deep origin, as was also suggested by the  $^{228}\text{Ra}_{\text{ex}}/^{226}\text{Ra}_{\text{ex}}$  ratios. In addition, the  $^{226}\text{Ra}_{\text{ex}}/\text{Ba}_{\text{ex}}$  ratios lower than the seawater ratio suggest fractionation between Ra and Ba during barite precipitation, a pattern that was also deduced from the ratios of suspended particles. Consequently, ratios found at 3200 m during the two sampling periods suggest that barite (or  $\text{Ba}_{\text{ex}}$ ) accumulates at the sea-floor with a  $^{226}\text{Ra}/\text{Ba}$  ratio slightly lower than  $2.3 \text{ dpm } \mu\text{mol}^{-1}$  (i.e. mean ratio at 3200 m is  $1.5 \text{ dpm } \mu\text{mol}^{-1}$ ).

## 5. CONCLUSION

Combining measurements of  $\text{Ba}_{\text{ex}}$ ,  $\text{Sr}_{\text{ex}}$ ,  $^{226}\text{Ra}_{\text{ex}}$  and  $^{228}\text{Ra}_{\text{ex}}$  in suspended and sinking particles and comparing their  $^{228}\text{Ra}_{\text{ex}}/^{226}\text{Ra}_{\text{ex}}$  and  $^{226}\text{Ra}_{\text{ex}}/\text{Ba}_{\text{ex}}$  ratios to those of seawater provide constraints on the origin and mode of formation of particulate  $\text{Ba}_{\text{ex}}$  (mostly barite) in the ocean.

1.  $^{228}\text{Ra}_{\text{ex}}/^{226}\text{Ra}_{\text{ex}}$  ratios of sinking particles suggest that barite exported to the deep sea has a mixed origin that varies with season. While particles settling to a depth of 1500 m in Spring and Summer can sometimes (but not always) have barite that is predominantly formed in shallow water, in agreement with Legeleux and Reyss (1996), barite found in winter samples appear to have been produced in deeper water. At 3200 m, settling particles have generally a larger proportion of barite produced in deep water. Barite production, therefore, is not restricted to shallow water but also seems to be significant at greater depth. The mechanism postulated by Ganeshram et al (2003), which invokes uptake of Ba by phytoplankton (with a surface Ra isotopic signature) and subsequent release in microenvironments of sinking particles, would produce a clear surface signal in the barite collected throughout the water column. Our data indicate that this proposed mechanism cannot be the only one that produces barite in the water

column. Deeper in the water column, barite must also be produced within microenvironments, which must act as a sink for seawater Ba.

2. The  $^{228}\text{Ra}_{\text{ex}}/^{226}\text{Ra}_{\text{ex}}$  ratios of suspended particles track closely that of seawater, confirming in situ formation of barite in deep water and minimal addition of barite by disaggregation of large sinking particles originating from the overlying mixed layer. The exchange of  $\text{Ba}_{\text{ex}}$  between suspended and sinking particles thus appear to mainly occur through the incorporation of barite produced in deep water into the settling flux.

3. The  $^{226}\text{Ra}_{\text{ex}}/\text{Ba}_{\text{ex}}$  ratio of suspended particles is higher than that of seawater above 200 m and lower below 700 m. Suspended particles in the upper water column have also high Sr content indicating the presence of celestite from acantharians. Taken together, these observations suggest (a) significant contribution of celestite dissolution to barite formation in the upper 500 m (b) preferential precipitation of Ba over Ra during barite formation.

## REFERENCES

Bacon M.P. and Edmond J.M. (1972) Barium at GEOSECS III in the Southwest Pacific. *Earth Planet. Sci. Lett.* **16**, 66-74.

Bacon M.P. and Anderson R. F. (1982) Distribution of thorium isotopes between dissolved and particulate forms in the deep sea. *Journal of Geophys. Res.* **87**, 2045-2056.

Bacon M.P., Huh C.-A., Fleer A.P. and Deuser W.G. (1985) Seasonality in the flux of natural radionuclides and plutonium in the deep Sargasso Sea. *Deep-Sea Res. I* **32** (3), 273-286.

Berkman P.A. and Ku T.-L. (1998)  $^{226}\text{Ra}/\text{Ba}$  ratios for dating Holocene biogenic carbonates in the Southern Ocean : preliminary evidence from Antarctic coastal mollusc shells. *Chem. Geology* **144**, 331-334.

- Bernstein R.E., Betzer P.R., Feely R.A., Byrne R.H., Lamb M.F. and Michaels A.F. (1987) Acantharian fluxes and strontium to chlorinity ratios in the North Pacific Ocean. *Science* **237**, 1490-1494.
- Bernstein R.E., Byrne R.H., Betzer P.R. and Greco A.M. (1992) Morphologies and transformations of celestite in seawater : the role of acantharians in strontium and barium geochemistry. *Geochim. Cosmochim. Acta* **56**, 3273-3279.
- Bernstein R.E., Byrne R.H. and Schijf J. (1998) Acantharians : a missing link in the oceanic biogeochemistry of barium. *Deep-Sea Res. II* **45**, 491-505.
- Bernstein R.E. and Byrne R.H. (2004) Acantharians and marine barite. *Mar. Chem.* **86**, 45-50.
- Bishop J.K.B., Edmond J.M., Ketten D.R., Bacon M.P. and Silker W.B. (1977) The chemistry, biology, and vertical flux of particulate matter from the upper 400 m of the equatorial Atlantic Ocean. *Deep-Sea Res.* **24**, 511-548.
- Bishop J.K.B., Ketten D. R. and Edmond J.M. (1978) The chemistry, biology, and vertical flux of particulate matter from the upper 400 m of the Cape Basin in the southeast Atlantic Ocean. *Deep-Sea Res.* **25**, 1121-1161.
- Bishop J.K.B. (1988) The barite-opal-organic carbon association in oceanic particulate matter. *Nature* **332**, 341-343.
- Broecker W.S., Li Y.H. and Cromwell J. (1967) Radium-226 and Radon-222 : Concentration in Atlantic and Pacific Oceans. *Science* **158**, 1307-1310.
- Broecker W.S., Goddard J. and Sarmiento J.L. (1976) The distribution of <sup>226</sup>Ra in the Atlantic Ocean. *Earth Planet. Sci. Lett.* **32**, 220-235.
- Chan L.H., Edmond J.M., Stallard R.F., Broecker W.S., Chung. Y.C., Weiss R.F. and Ku T.L. (1976) Radium and barium at GEOSECS stations in the Atlantic and Pacific. *Earth Planet. Sci. Lett.* **32**, 258-267.

- Chan L.H., Drummond D., Edmond J.M. and Grant B. (1977) On the barium data from the Atlantic GEOSECS expedition. *Deep-Sea Res.* **24**, 613-649.
- Chow T.J. and Goldberg E.D. (1960) On the marine geochemistry of barium. *Geochim. Cosmochim. Acta* **20**, 192-198.
- Chung Y.-C. (1974) Radium-226 and Ra-Ba relationships in Antarctic and Pacific waters. *Earth Planet. Sci. Lett.* **23**, 125-135.
- Chung Y.-C. (1976) A deep  $^{226}\text{Ra}$  maximum in the northeast Pacific. *Earth Planet. Sci. Lett.* **32**, 249-257.
- Chung Y.-C. and Craig H. (1980)  $^{226}\text{Ra}$  in the Pacific Ocean. *Earth Planet. Sci. Lett.* **49**, 267-292.
- Church T.M. and Wolgemuth K. (1972) Marine barite saturation. *Earth Planet. Sci. Lett.* **15**, 35-44.
- Conte M.H., Ralph N. and Ross E.H. (2001) Seasonal and interannual variability in deep ocean particles fluxes at the Oceanic Flux Program (OFP)/ Bermuda Atlantic Time Series (BATS) site in the western Sargasso Sea near Bermuda. *Deep-Sea Res.* **48**, 1471-1505.
- Dehairs F., Chesselet R. and Jedwab J. (1980) Discrete suspended particles of barite and the barium cycle in the open ocean. *Earth Planet. Sci. Lett.* **49**, 528-550.
- Dehairs F., Goeyens L., Stroobants N., Bernard P., Goyet C., Poisson A. and Chesselet R. (1990) On suspended barite and the oxygen minimum in the Southern Ocean. *Global Biogeochem. Cycles* **4** (1), 85-102.
- Dehairs F., Stroobants N. and Goeyens L. (1991) Suspended barite as tracer of biological activity in the Southern Ocean. *Mar. Chem.* **35**, 399-410.
- Dehairs F., Baeyens W. and Goeyens, L. (1992) Accumulation of suspended barite at mesopelagic depths and export production in the Southern Ocean. *Science* **258**, 1332-1335.

- Dickey T., Zedler S., Frye D., Jannasch H., Manov D., Sigurdson D., McNeil J.D., Dobeck L., Yu X., Gilboy T., Bravo C., Doney S.C., Siegel D.A. and Nelson N. (2001) Physical and biogeochemical variability from hours to years at the Bermuda Testbed Mooring site: June 1994 – March 1998. *Deep-Sea Res. II* **48**, 2105-2140.
- Dymond J., Suess E. and Lyle M. (1992) Barium in deep-sea sediment : A geochemical proxy for paleoproductivity. *Paleoceanography* **7** (2), 163-181.
- Foster D.A., Staubwasser M. and Henderson G.M. (2004)  $^{226}\text{Ra}$  and Ba concentrations in the Ross Sea measured with multicollector ICP mass spectrometry. *Mar. Chem.* **87**, 59-71.
- François R., Honjo S., Manganini S.J. and Ravizza G.E. (1995) Biogenic barium fluxes to the deep sea : Implications for paleoproductivity reconstruction. *Global Biogeochem. Cycles* **9** (2), 289-303.
- Ganeshram R.S., François R., Commeau J. and Brown-Leger S.L. (2003) An experimental investigation of barite formation in seawater. *Geochim. Cosmochim. Acta.* **67** (14), 2599-2605.
- Gingele F. and Dahmke A. (1994) Discrete barite particles and barium as tracers of paleoproductivity in South Atlantic sediments. *Paleoceanography* **9** (1), 151-168.
- Jacquet S.H.M., Dehairs F. and Rintoul S. (2004) A high resolution transect of dissolved barium in the Southern Ocean. *Geophys. Res. Lett.* **31**, L14301, doi :10.1029/2004GL020016.
- Joyce T. M. and Robbins P. (1996) The long-term hydrographic record at Bermuda. *J. Climate* **9**, 3121-3131.
- Kaufman A., Trier R.M., Broecker W.S., Feely H.W. (1973) Distribution of  $^{228}\text{Ra}$  in the world ocean. *Journal of geophys. Res.* **78** (36), 8827-8848.
- Kim G., Hussein N. and Church T. (2003) Tracing the advection of organic carbon into the subsurface Sargasso Sea using  $^{228}\text{Ra}/^{226}\text{Ra}$  tracer. *Geophys. Res. Lett.* **30** (16), 1874, doi:10.1029/2003GL017565.

- Krishnaswami S., Sarin M.M. and Somayajulu B.L.K. (1981). Chemical and radiochemical investigations of surface and deep particles in the Indian Ocean. *Earth Planet. Sci. Lett.* **54**, 81-96.
- Ku T.-L. and Lin M.-C. (1976)  $^{226}\text{Ra}$  distribution in the Antarctic Ocean. *Earth Planet. Sci. Lett.* **32**, 236-248.
- Ku T.-L., Huh C.-A. and Chen P.S. (1980) Meridional distribution of  $^{226}\text{Ra}$  in the eastern Pacific along GEOSECS cruise tracks. *Earth Planet. Sci. Lett.* **49**, 293-308.
- Legeleux F. and Reyss J.-L. (1996) Ra-228/ Ra-226 activity ratio in oceanic settling particles : Implications regarding the use of barium as a proxy for paleoproductivity reconstruction. *Deep-Sea Res. I* **43** (11-12), 1857-1863.
- Li Y.H., Ku T.L., Mathieu G.G. and Wolgemuth K. (1973) Barium in the Antarctic Ocean and implications regarding the marine Geochemistry of Ba and  $^{226}\text{Ra}$ . *Earth Planet. Sci. Lett.* **19**, 352-358.
- Li Y.H., Feely H.W. and Toggweiler J.R. (1980)  $^{228}\text{Ra}$  and  $^{228}\text{Th}$  concentrations in GEOSECS Atlantic surface waters. *Deep-sea Research* **27A**, 545-55.
- Mackenzie F.T. (1964) Strontium content and variable strontium-chlorinity relationship of Sargasso Sea water. *Science* **146**, 517-518.
- Michaels A.F. (1988) Vertical distribution and abundance of Acantharia and their symbionts. *Marine Biology* **97**, 559-569.
- Michaels A.F., Caron D.A., Swanberg N.R., Howse F.A. and Michaels C. (1995) Planktonic sarcodines (Acantharia, Radiolaria, Foraminifera) in surface waters near Bermuda : abundance, biomass and vertical flux. *Journal of Plankton Res.* **17** (1), 131-163.
- Monnin C., Jeandel C., Cattaldo T. and Dehairs F. (1999) The marine barite saturation state of the world's oceans. *Mar. Chem.* **65**, 253-261.

Moore W.S. and Reid D.F. (1973) Extraction of radium from natural waters using manganese-impregnated acrylic fibers. *Journal of Geophys. Res.* **78**, 8880-8886.

Moore W.S., Key R.M. and Sarmiento J. L. (1985) Techniques for precise mapping of  $^{226}\text{Ra}$  and  $^{228}\text{Ra}$  in the ocean. *Journal of Geophys. Res.* **90**, 6983-6995.

Moore W.S. (1987) Radium 228 in the South Atlantic Bight. *Journal of Geophys. Res.* **92**, 5177-5190.

Moore W.S. and Dymond J. (1991) Fluxes of Ra-226 and barium in the Pacific Ocean : The importance of boundary processes. *Earth Planet. Sci. Lett.* **107**, 55-68.

Nürnberg C.C., Bohrmann G. and Schlüter M. (1997) Barium accumulation in the Atlantic sector of the Southern Ocean : Results from 190,000-year records. *Paleoceanography* **12** (4), 594-603.

Paytan A., Kastner M. and Chavez F.P. (1996a) Glacial to Interglacial fluctuations in productivity in the equatorial Pacific as indicated by marine barite. *Science* **274**, 1355-1357.

Paytan A., Moore W.S. and Kastner M. (1996b) Sedimentation rate as determined by  $^{226}\text{Ra}$  activity in marine barite. *Geochim. Cosmochim. Acta* **60** (22), 4313-4319.

Reyss J.-L., Schmidt S., Legeleux F. and Bonte P. (1995) Large, low background well-type detectors for measurements of environmental radioactivity. *Nucl. Inst. and Meth. A* **357**, 391-397.

Rhein M. and Schlitzer R. (1988) Radium-226 and barium sources in the deep East Atlantic, *Deep-Sea Res.* **35** (9), 1499-1510.

Rushdi A., McManus J. and Collier. R. (2000) Marine barite and celestite saturation in seawater. *Mar. Chem.* **69**, 19-31.

Schmitz B. (1987) Barium, equatorial high productivity, and the northward wandering of the Indian continent. *Paleoceanography* **2** (1), 63-77.

Sherrell R.M. and Boyle E. A. (1992) The trace metal composition of suspended particles in the oceanic water column near Bermuda. *Earth Planet. Sci. Lett.* **111**, 155-174.

Stroobants N., Dehairs F., Goeyens L., Vanderheijden N. and van Grieken R. (1991) Barite formation in the Southern Ocean water column. *Mar. Chem.* **35**, 411-421.

Staubwasser M., Henderson G.M., Berkman P.A. and Hall B.L. (2004) Ba, Ra, Th, and U in marine mollusc shells and the potential of  $^{226}\text{Ra}/\text{Ba}$  dating of Holocene marine carbonate shells. *Geochim. Cosmochim. Acta.* **68** (1), 89-100.

Steinberg D. K., Carlson C.A., Bates N.R., Johnson R.J., Michaels A.F. and Knap A.H. (2001) Overview of the U. S. JGOFS Bermuda Atlantic Time-Series Study (BATS): A decade look at ocean biology and biogeochemistry. *Deep-Sea Res.* **48**, 1405-1448.

Talley L. (1996) North Atlantic circulation and variability, reviewed for the CNLS conference. *Physica D*, 625-646.

Taylor S.R. and McLennan S.M. (1985) *The continental crust : its composition and evolution*. Blackwell, Cambridge, Massachusetts.

van Beek P. and Reyss J.-L. (2001)  $^{226}\text{Ra}$  in marine barite : new constraints on supported  $^{226}\text{Ra}$ . *Earth Planet. Sci. Lett.* **187**, 147-161.

van Beek P., Reyss J.-L., Gersonde R., Paterne M., Rutgers van der Loeff M. and Kuhn G. (2002)  $^{226}\text{Ra}$  in barite : absolute dating of Holocene Southern Ocean sediments and reconstruction of sea-surface reservoir ages. *Geology* **30** (8), 731-734.

van Beek P., Reyss J.-L., DeMaster D. and Paterne M. (2004)  $^{226}\text{Ra}$ -in marine barite : Relationship with carbonate dissolution and sediment focusing in the equatorial Pacific. *Deep-Sea Research I* **51**, 235-261.

Wolgemuth K. and Broecker W.S. (1970) Barium in sea water. *Earth Planet. Sci. Lett.* **8**, 372-378.

*Acknowledgements* - We are grateful to the crew and captain of Weatherbird II. We thank Larry Ball and David Schneider at the ICP/MS of WHOI, USA; Valérie Olive at the ICP/MS of East Kilbride, Scotland, UK; Frédéric Candaudap at the ICP/MS of Observatoire Midi Pyrénées, Toulouse; Carole Causserand at the atomic spectrophotometry, Observatoire Midi Pyrénées, Toulouse. We are grateful to John C. Weber for his help with the sinking particles samples. We also thank Alan Fleer, Susan Brown-Léger and Bernhard Peucker-Ehrenbrink at WHOI. We thank Charlotte Riccio, Thierry Sampieri and Jean-Louis Saury at the underground laboratory of Modane as well as Sophie Ayrault, Serge Boiziau at the Laboratoire Pierre Süe, Saclay. We are grateful to Paul Lethaby and Christine Pequignet (BBSR) for providing the CTD data. This work was supported by a Lavoisier fellowship given by the French Ministry of Foreign Affairs and by the Woods Hole Oceanographic Institution.

### **Figure caption**

Fig. 1 : Hydrology at the OFP site. Profiles of salinity, potential temperature, oxygen and density are reported. Arrows indicate the depths of sample collection (suspended particles and seawater).

Fig. 2 : Ba,  $^{226}\text{Ra}$  and  $^{228}\text{Ra}$  profiles in seawater.

Fig. 3 : The upper panels show Ba,  $^{226}\text{Ra}$  and  $^{228}\text{Ra}$  profiles in suspended particles while the lower panels show excess Ba,  $^{226}\text{Ra}$  and  $^{228}\text{Ra}$  profiles in suspended particles (that is, total contents corrected for the lithogenic fraction). In the upper panel, open circles represent total Ba concentrations, total  $^{226}\text{Ra}$  and  $^{228}\text{Ra}$  activities, respectively whereas solid circles represent the concentrations associated with the lithogenic fraction. Arrows on the lower panel indicate the depths where no significant  $\text{Ba}_{\text{ex}}$  or  $^{228}\text{Ra}_{\text{ex}}$  activities were measured in the suspended particles.

Fig. 4 :  $^{228}\text{Ra}_{\text{ex}}/^{226}\text{Ra}_{\text{ex}}$  ratios in suspended particles (solid squares) reported together with the ratios found in seawater (open circles). Arrows indicate the depths where no significant  $^{228}\text{Ra}_{\text{ex}}$  were measured in the suspended particles. As a comparison, the shaded bars represents the range of values found in sinking particles (at 1500 m and 3200 m, respectively).

Fig. 5 : Left panel :  $^{226}\text{Ra}/\text{Ba}$  ratios in seawater (open circles) reported together with  $^{226}\text{Ra}_{\text{ex}}/\text{Ba}_{\text{ex}}$  ratios in suspended particles (closed squares). Right panel : Sr content measured in suspended particles. Solid circles represent the total Sr content (corrected for the Sr associated with sea-salt) while open circles consist in the non-carbonate Sr.

Fig. 6 :  $^{228}\text{Ra}_{\text{ex}}/^{226}\text{Ra}_{\text{ex}}$  ratios in sinking particles collected with sediment traps reported versus water depth (upper panels) and versus time (lower panels). Solid symbols represent the ratios found in sinking particles whereas open circles represent the seawater ratios. Results obtained on samples collected in 1988-1989 are reported on the left panel, while those from samples collected in 1999-2000 are reported on the right panel. Width of the plots on the lower panels indicates sampling duration.

### Left panels

Solid squares : 19 march - 17 may 1988 (58 days collection)  
Up triangles : 13 july - 13 september 1988 (61 days collection)  
Down triangles : 15 november 1988 - 1 february 1989 (76 days collection)  
Diamonds : 1 february - 4 april 1989 (61 days collection)

### Right panels

Diamonds : 10 december 1999 - 25 december 1999 (15 days collection)  
Solid squares : 23 march 2000 - 5 april 2000 (14 days collection)  
Up triangles : 5 june 2000 - 20 june 2000 (15 days collection)  
Down triangles : 5 september 2000 - 20 september 2000 (15 days collection)

Fig. 7 :  $^{226}\text{Ra}_{\text{ex}}/\text{Ba}_{\text{ex}}$  ratios in sinking particles reported versus time. The depth of the sediment trap is shown on the plots. Legend is same as Fig. 6. The shaded area represents the range of values found in seawater (Fig. 5). Width of the plots indicates sampling duration.

Fig. 8 : Left panel :  $^{228}\text{Ra}_{\text{ex}}/^{226}\text{Ra}_{\text{ex}}$  ratio expected in suspended particles considering that the particles acquire the seawater ratio of surface waters (solid symbols; initial ratio of 0.38) or subsurface (open symbols; initial ratio of 0.30) and that they settle at a rate of 1000 m/ y (circles), 300 m/ y (squares) or 40 m/ y (diamonds). Ratios measured in the suspended particles are shown in grey with their associated error bars. Right panel :  $^{228}\text{Ra}_{\text{ex}}$  activities expected in suspended particles collected below 250 m as deduced from the  $^{226}\text{Ra}_{\text{ex}}$  activities measured in each sample and considering that the particles acquired the seawater  $^{228}\text{Ra}/^{226}\text{Ra}$  ratio in surface waters (solid symbols; initial ratio of 0.38) or subsurface (open symbols; initial ratio of 0.30). Vertical profiles were computed considering settling rates of 300 m/ y (squares) and 1000 m / y (circles). The dotted line represents the expected values in case  $\text{Ba}_{\text{ex}}$  incorporates the seawater ratio throughout the water column.  $^{228}\text{Ra}_{\text{ex}}$  activities measured in suspended particles are also reported (solid squares with error bars).



Table 1 : Results of measurements conducted in seawater

depth m	Ba nmol kg <sup>-1</sup> (± 2 %)	<sup>226</sup> Ra dpm/ 100 kg	<sup>228</sup> Ra dpm/ 100 kg	<sup>228</sup> Ra/ <sup>226</sup> Ra	<sup>226</sup> Ra/Ba dpm μmol <sup>-1</sup>
20	43.90	8.71 ± 0.12	3.42 ± 0.16	0.39 ± 0.02	1.98 ± 0.05
70	44.32	9.21 ± 0.18	3.16 ± 0.23	0.34 ± 0.03	2.08 ± 0.06
120	44.09	7.82 ± 0.19	3.26 ± 0.27	0.42 ± 0.04	1.77 ± 0.06
170	44.84	8.96 ± 0.17	2.77 ± 0.22	0.31 ± 0.02	2.00 ± 0.06
250	44.80	8.16 ± 0.14	2.67 ± 0.20	0.33 ± 0.03	1.82 ± 0.05
350	45.00				
450	49.80	8.20 ± 0.22	2.01 ± 0.24	0.25 ± 0.03	1.65 ± 0.06
550	43.21				
700	47.12	10.98 ± 0.31	0.56 ± 0.21	0.05 ± 0.02	2.33 ± 0.08
1000	50.52	11.67 ± 0.21	0.30 ± 0.21	0.03 ± 0.02	2.31 ± 0.06
1600	46.92	11.21 ± 0.17	0.16 ± 0.12	0.01 ± 0.01	2.39 ± 0.06
2380	56.87	12.94 ± 0.12	0.31 ± 0.09	0.02 ± 0.01	2.28 ± 0.05
3250	60.48				
3700	63.81	12.49 ± 0.16	0.33 ± 0.08	0.03 ± 0.01	1.96 ± 0.05
4000	70.37	15.20 ± 0.16	0.52 ± 0.09	0.03 ± 0.01	2.16 ± 0.05
4250	78.82	17.50 ± 0.17	0.81 ± 0.09	0.05 ± 0.01	2.22 ± 0.05

Table 2 : Results of measurements conducted in suspended particles (in situ pumps)

depth m	$^{226}\text{Ra}$		$^{228}\text{Ra}$		$^{232}\text{Th}$	lithogenic $^{238}\text{U}^1$	$^{226}\text{Ra}_{\text{ex}}$		$^{228}\text{Ra}_{\text{ex}}$		$^{228}\text{Ra}_{\text{ex}} / ^{226}\text{Ra}_{\text{ex}}$	
	dpm/ 100 kg		dpm/ 100 kg		dpm/ 100 kg ( $\pm 4\%$ )	dpm/ 100 kg ( $\pm 4\%$ )	dpm/ 100 kg		dpm/ 100 kg			
20	0.090	$\pm 0.001$	0.0710	$\pm 0.0160$	n.m.	–	–	–	–	–	–	–
70	0.060	$\pm 0.005$	0.0170	$\pm 0.0040$	0.00053	0.00042	0.060	$\pm 0.0055$	0.0165	$\pm 0.0039$	0.276	$\pm 0.071$
120	0.056	$\pm 0.004$	0.0130	$\pm 0.0040$	0.00029	0.00023	0.056	$\pm 0.0046$	0.0127	$\pm 0.0039$	0.228	$\pm 0.073$
170	0.031	$\pm 0.003$	0.0110	$\pm 0.0030$	0.00015	0.00012	0.031	$\pm 0.0032$	0.0109	$\pm 0.003$	0.351	$\pm 0.104$
300	0.040	$\pm 0.002$	0.0110	$\pm 0.0020$	0.00035	0.00028	0.040	$\pm 0.0025$	0.0107	$\pm 0.0020$	0.268	$\pm 0.053$
450	0.027	$\pm 0.001$	0.0060	$\pm 0.0010$	0.00021	0.00017	0.027	$\pm 0.0015$	0.0058	$\pm 0.0010$	0.216	$\pm 0.039$
700	0.024	$\pm 0.001$	0.0020	$\pm 0.0010$	0.00043	0.00034	0.024	$\pm 0.0014$	0.0016	$\pm 0.0008$	0.066	$\pm 0.034$
1420	0.015	$\pm 0.001$	0.0004	$\pm 0.0004$	0.00058	0.00046	0.015	$\pm 0.0011$	0		0	
1670	0.010	$\pm 0.001$	0.0008	$\pm 0.0003$	0.00033	0.00026	0.010	$\pm 0.0010$	0.0005	$\pm 0.0002$	0.048	$\pm 0.019$
2380	0.007	$\pm 0.001$	0.0005	$\pm 0.0002$	0.00053	0.00042	0.007	$\pm 0.0008$	0		0	
4000	0.005	$\pm 0.001$	0.0018	$\pm 0.0004$	0.00532	0.00425	0.001	$\pm 0.0001$	0		0	
4250	0.009	$\pm 0.001$	0.0030	$\pm 0.0006$	0.00365	0.00292	0.006	$\pm 0.0005$	0		0	

Table 2 (following)

depth m	Ba	lithogenic Ba <sup>2</sup>	Ba <sub>ex</sub>	$^{226}\text{Ra}_{\text{ex}} / \text{Ba}_{\text{ex}}$		Sr <sup>3</sup>	non-carbonate Sr <sup>4</sup>
	nmol kg <sup>-1</sup> ( $\pm 4\%$ )	nmol kg <sup>-1</sup> ( $\pm 4\%$ )	nmol kg <sup>-1</sup> ( $\pm 4\%$ )	dpm $\mu\text{mol}^{-1}$		nmol kg <sup>-1</sup> ( $\pm 10\%$ )	nmol kg <sup>-1</sup> ( $\pm 10\%$ )
20	0.048	–	–	–	–	0.302	0.248
70	0.243	0.008	0.235	2.54	$\pm 0.26$	0.508	0.086
120	0.150	0.004	0.146	3.83	$\pm 0.35$	0.421	0.257
170	0.116	0.002	0.114	2.71	$\pm 0.30$	0.183	0.122
300	0.177	0.005	0.172	2.31	$\pm 0.17$	0.211	0.128
450	0.127	0.003	0.124	2.17	$\pm 0.15$	0.164	0.101
700	0.119	0.007	0.112	2.10	$\pm 0.15$	0.155	0.096
1420	0.107	0.009	0.098	1.49	$\pm 0.13$	0.152	0.088
1670	0.074	0.005	0.069	1.41	$\pm 0.16$	0.109	0.069
2380	0.059	0.008	0.050	1.33	$\pm 0.16$	0.100	0.058
4000	0.057	0.083	0	0		0.102	0.074
4250	0.070	0.057	0.014	4.78	$\pm 0.41$	0.098	0.048

<sup>1</sup> derived from the  $^{232}\text{Th}$  activities considering a U/Th ratio of 0.8 (dpm/dpm) after Taylor and McLennan (1985)

<sup>2</sup> derived from the  $^{232}\text{Th}$  activities using Ba/ $^{232}\text{Th}$  of the upper crust after Taylor and McLennan (1985)

<sup>3</sup> Sr content corrected for Sr associated with sea-salt

<sup>4</sup> Sr content further corrected for Sr associated with CaCO<sub>3</sub>

n.m. : not measured

Table 3. : Results of measurements conducted in sinking particles (sediment traps)

sample	depth m	sampling duration d	total flux mg m <sup>-2</sup> d <sup>-1</sup>	<sup>226</sup> Ra		<sup>228</sup> Ra		<sup>232</sup> Th <sup>1</sup>	<sup>232</sup> Th <sup>2</sup>	<sup>238</sup> U <sup>3</sup>
				dpm g <sup>-1</sup>	±	dpm g <sup>-1</sup>	±	dpm g <sup>-1</sup> (± 5%)	dpm g <sup>-1</sup> (± 3%)	dpm g <sup>-1</sup>
march-may1988	1500	58	59.8	11.46	± 0.22	0.79	± 0.11	0.33	—	0.26
march-may1988	3200	58	49.3	8.56	± 0.17	0.67	± 0.12	0.51	—	0.41
jul.-sept. 1988	1500	61	31.7	9.30	± 0.19	0.85	± 0.13	0.60	—	0.48
jul.-sept. 1988	3200	61	36.4	7.96	± 0.23	0.77	± 0.17	0.56	—	0.45
nov.1988-jan. 1989	1500	76	29.2	10.14	± 0.23	0.91	± 0.21	n.m.	0.65	0.52
nov.1988-jan. 1989	3200	76	37.8	7.66	± 0.22	0.69	± 0.2	0.73	—	0.58
jan.-april 1989	1500	61	50.9	9.24	± 0.20	0.77	± 0.17	0.57	—	0.46
jan.-april 1989	3200	61	58.4	7.58	± 0.15	0.87	± 0.15	0.62	—	0.50
dec. 1999	1500	15	29.7	9.30	± 0.51	1.28	± 0.42	—	0.55	0.44
dec. 1999	3200	15	24.8	6.76	± 0.54	0.53	± 0.25	—	0.81	0.65
march 2000	1500	14	57.9	7.21	± 0.41	2.53	± 0.38	—	n.m.	n.m.
march 2000	3200	14	61.2	3.04	± 0.09	0.57	± 0.07	—	0.56	0.45
june 2000	1500	15	28.7	8.13	± 0.73	1.04	± 0.57	—	0.58	0.47
june 2000	3200	15	19.9	10.10	± 0.87	0.39	± 0.28	—	0.64	0.51
sept. 2000	1500	15	34.6	6.30	± 0.29	1.38	± 0.30	—	0.62	0.50
sept. 2000	3200	15	35.1	5.95	± 0.49	1.23	± 0.39	—	0.64	0.51

Table 3. (following)

depth m	<sup>226</sup> Ra <sub>ex</sub>		<sup>228</sup> Ra <sub>ex</sub>		<sup>228</sup> Ra <sub>ex</sub> <sup>o</sup>		<sup>228</sup> Ra <sub>ex</sub> <sup>o</sup> / <sup>226</sup> Ra <sub>ex</sub>		Ba <sub>ex</sub>	<sup>226</sup> Ra <sub>ex</sub> /Ba <sub>ex</sub>	Ba <sub>ex</sub> flux
	dpm g <sup>-1</sup>	±	dpm g <sup>-1</sup>	±	dpm g <sup>-1</sup>	±		±	ppm (± 3%)	dpm/μmol	μmol m <sup>-2</sup> d <sup>-1</sup>
1500	11.20	± 0.60	0.46	± 0.07	2.37	± 0.35	0.21	± 0.044	433	3.55 ± 0.22	0.19
3200	8.15	± 0.44	0.16	± 0.03	0.82	± 0.15	0.10	± 0.027	504	2.22 ± 0.14	0.18
1500	8.82	± 0.48	0.25	± 0.04	1.24	± 0.20	0.14	± 0.032	296	4.09 ± 0.25	0.07
3200	7.51	± 0.43	0.21	± 0.05	1.04	± 0.24	0.14	± 0.044	799	1.29 ± 0.08	0.21
1500	9.62	± 0.36	0.26	± 0.06	1.20	± 0.28	0.12	± 0.041	872	1.52 ± 0.07	0.19
3200	7.08	± 0.41	0		0		0		798	1.22 ± 0.08	0.22
1500	8.78	± 0.48	0.20	± 0.05	0.92	± 0.21	0.11	± 0.034	716	1.69 ± 0.10	0.27
3200	7.08	± 0.38	0.25	± 0.04	1.16	± 0.21	0.16	± 0.041	406	2.40 ± 0.15	0.17
1500	8.86	± 0.55	0.73	± 0.24	1.02	± 0.34	0.12	± 0.054	908	1.34 ± 0.09	0.20
3200	6.11	± 0.52	0		0		0		825	1.02 ± 0.09	0.15
1500	—		—		—		—		—	—	—
3200	2.59	± 0.11	0		0		0		666	0.53 ± 0.03	0.30
1500	7.66	± 0.73	0.46	± 0.25	0.58	± 0.32	0.08	± 0.059	1042	1.01 ± 0.10	0.22
3200	9.59	± 0.87	0		0		0		654	2.01 ± 0.19	0.09
1500	5.80	± 0.32	0.76	± 0.17	0.98	± 0.22	0.17	± 0.053	723	1.10 ± 0.07	0.18
3200	5.44	± 0.48	0.59	± 0.19	0.73	± 0.24	0.13	± 0.061	719	1.04 ± 0.10	0.18

<sup>1</sup> Neutron Activation

<sup>2</sup> ICP/MS

<sup>3</sup> lithogenic <sup>238</sup>U determined from <sup>232</sup>Th; ± 3% for ICP/MS and ± 5% for neutron activation

n.m. : not measured

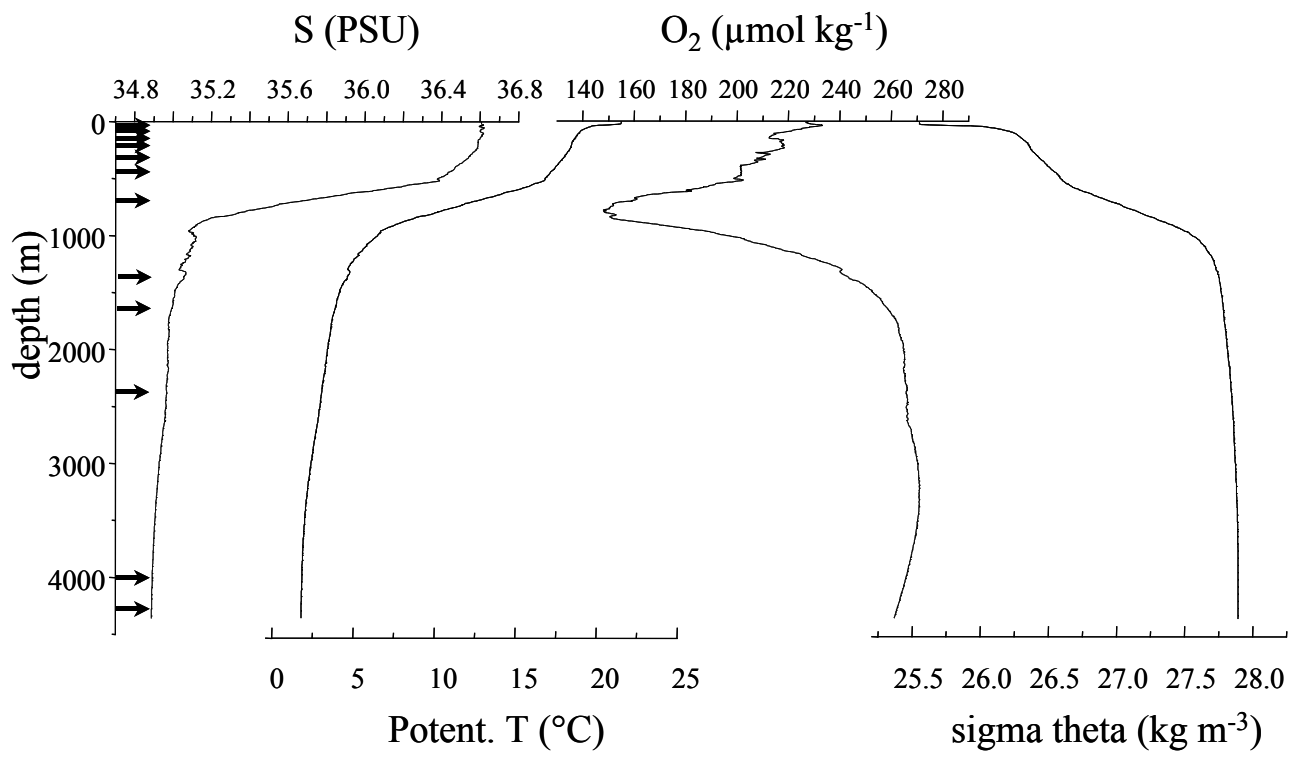
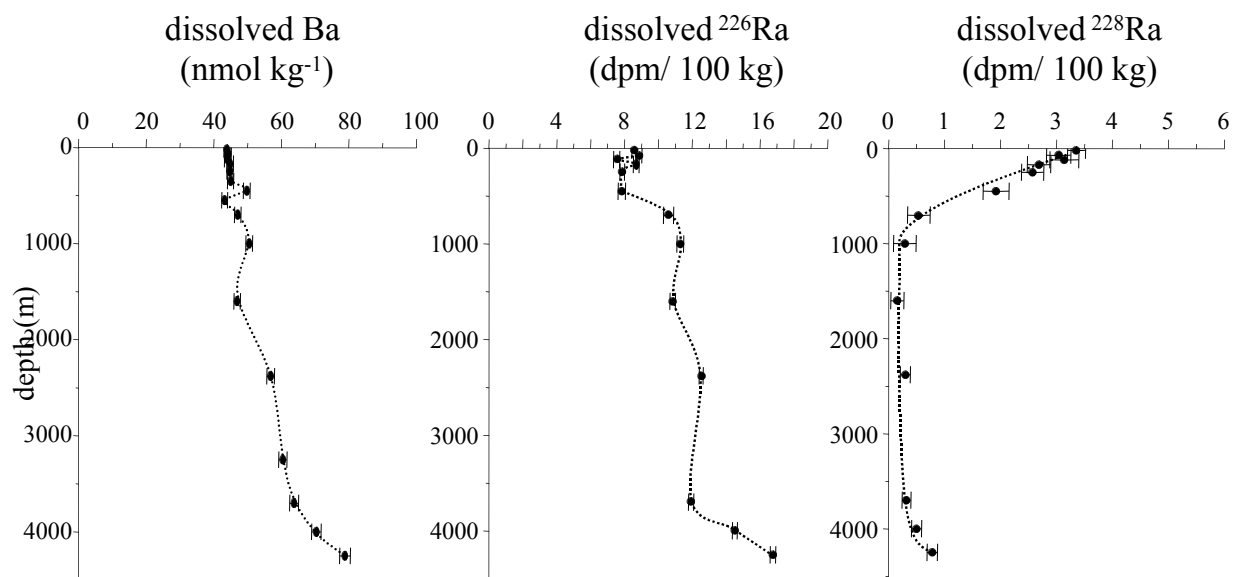
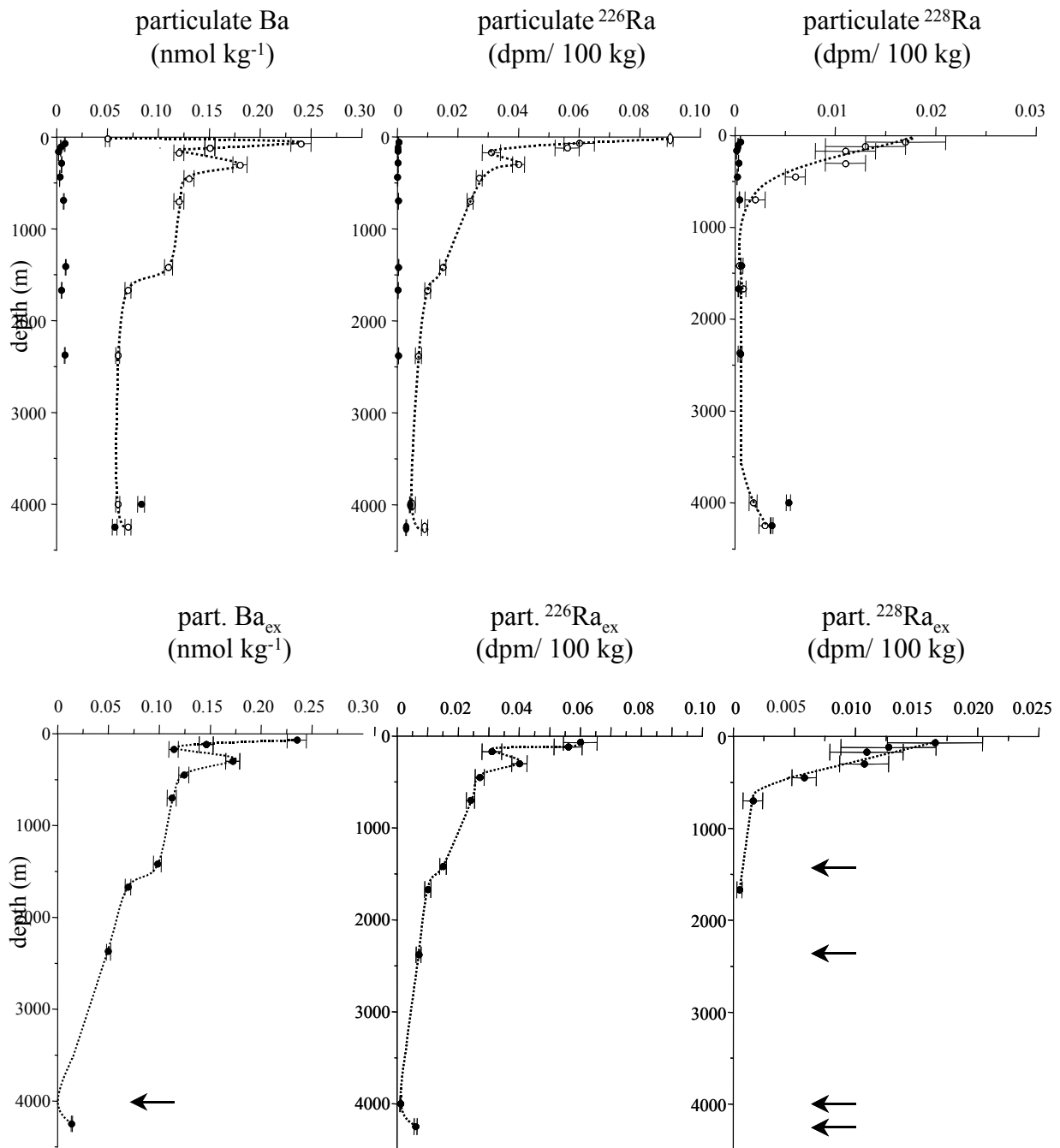


Fig. 1



**Fig. 2**



**Fig. 3**

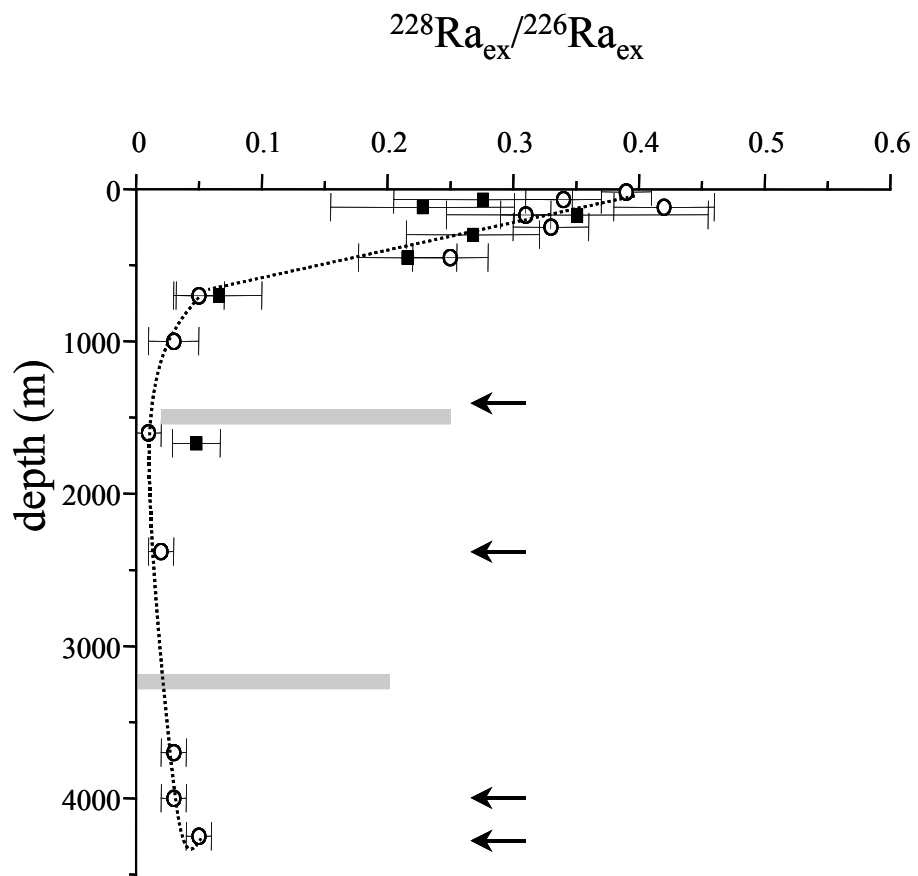


**Fig. 4**

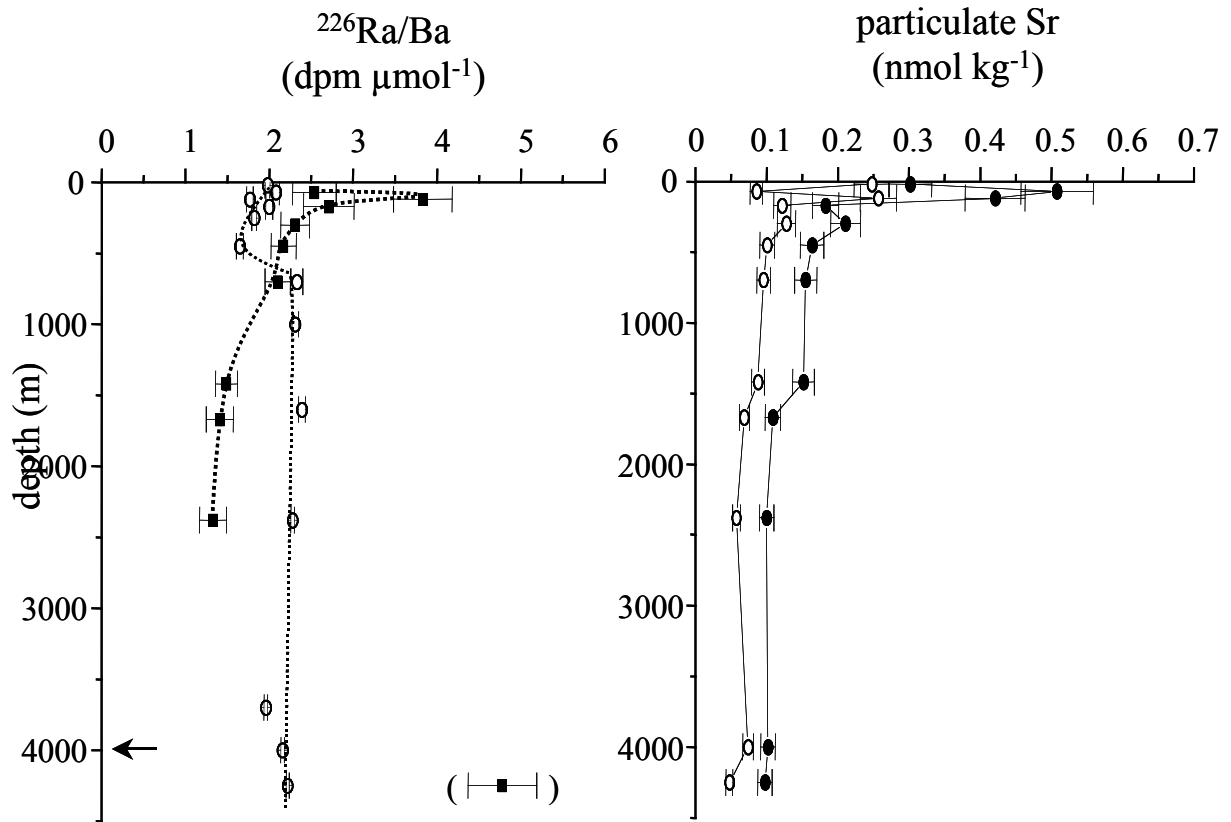
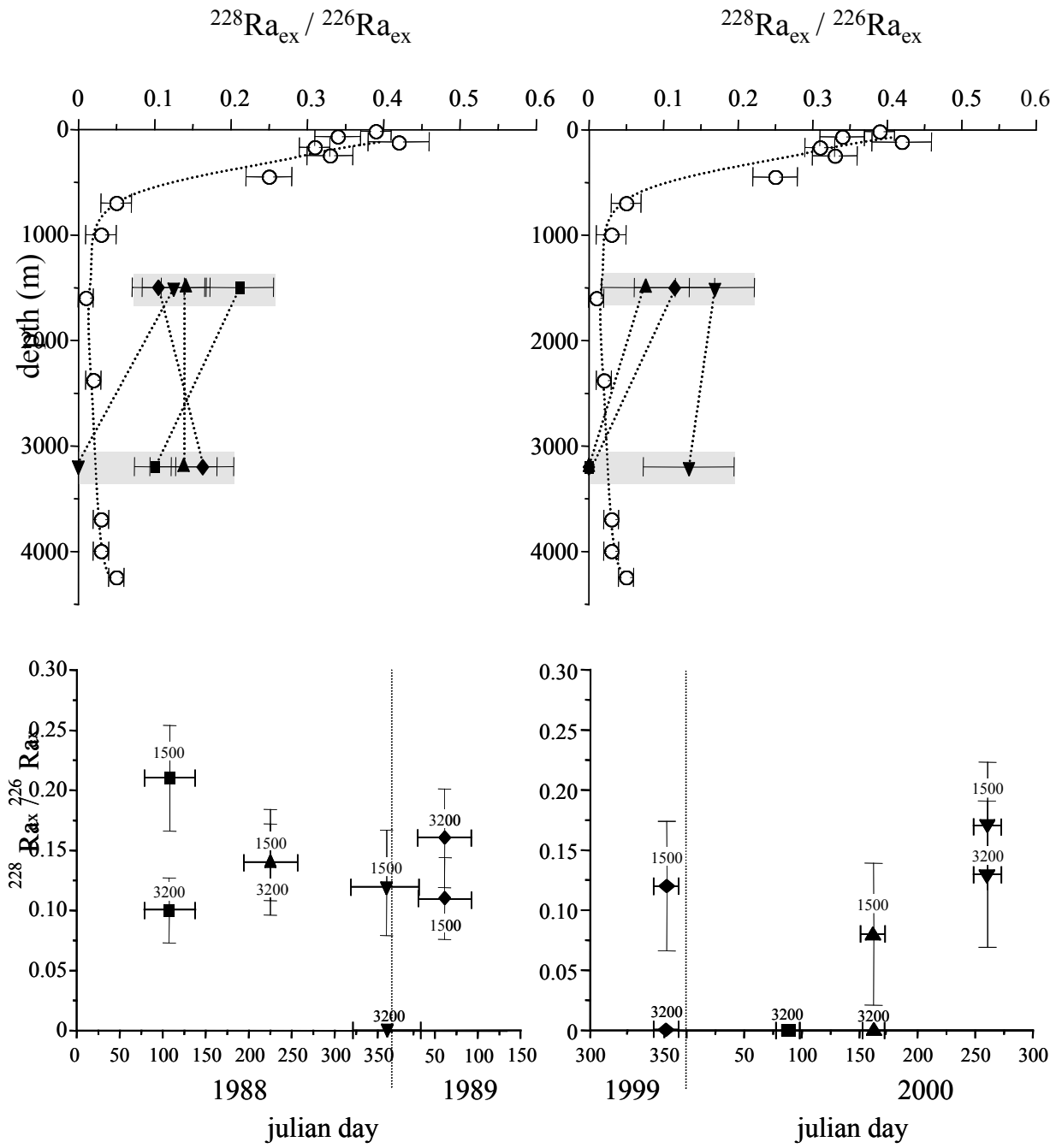
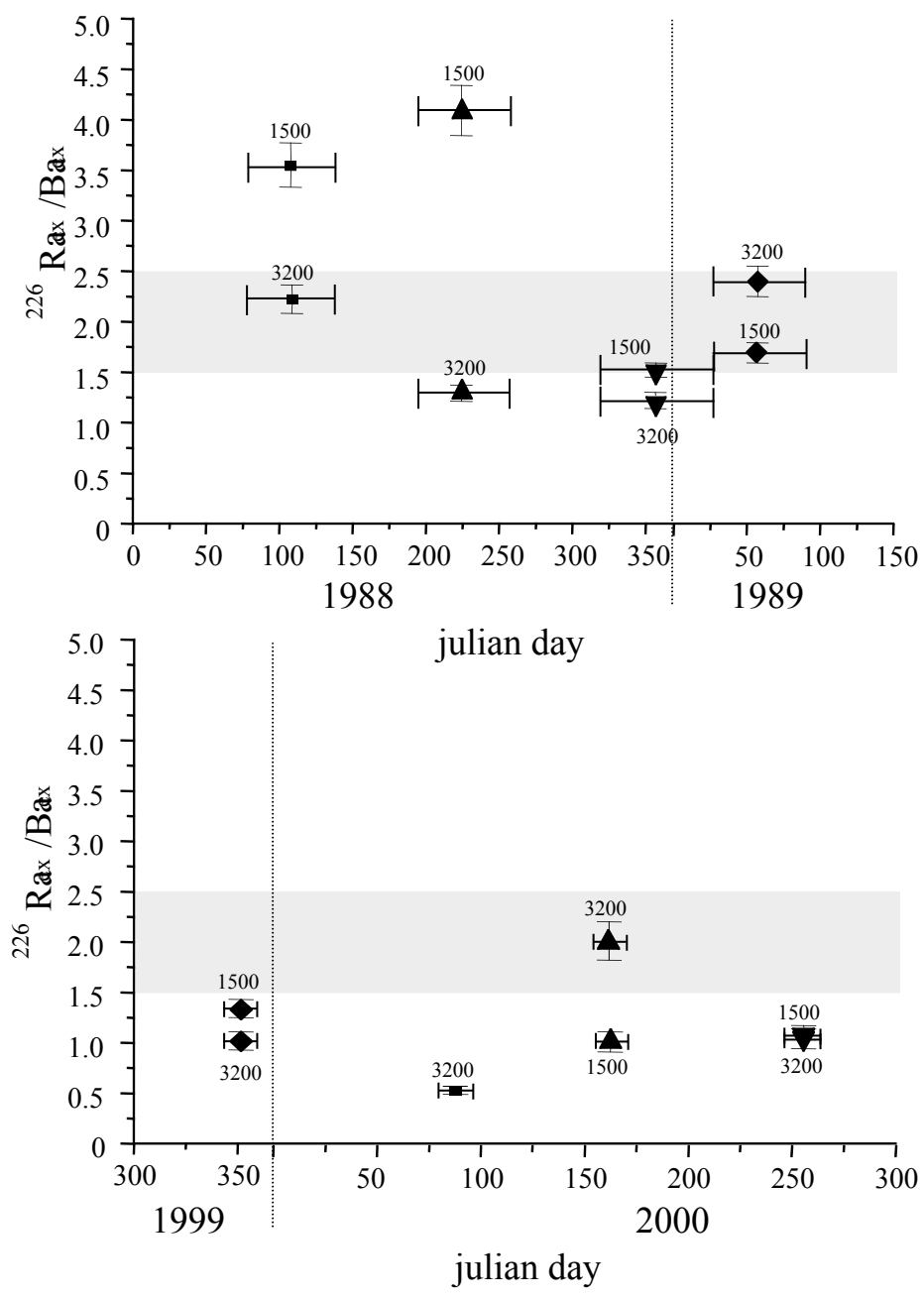


Fig. 5



**Fig. 6**



**Fig. 7**

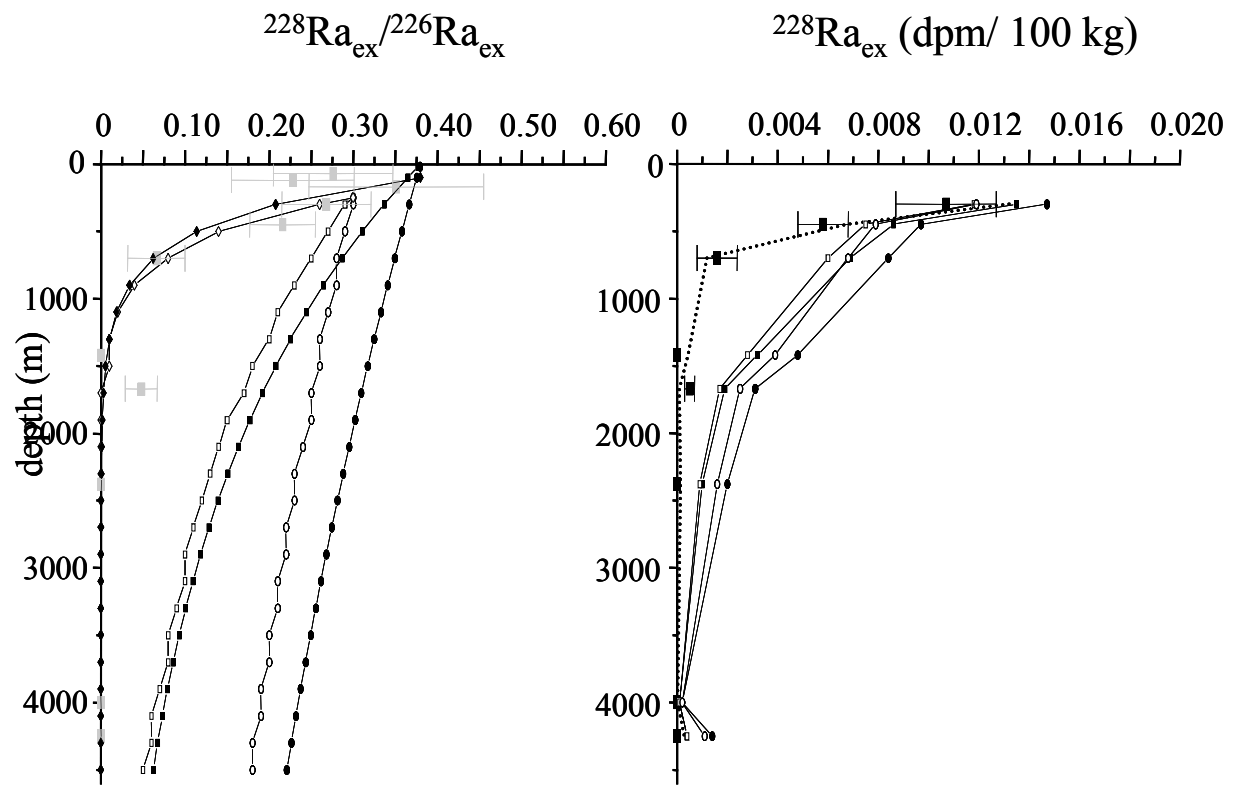


**Fig. 8**